NAVAL POSTGRADUATE SCHOOL
MONTEREY, CALIFORNIA

THESIS

ANALYSIS OF HARDWARE IMPLEMENTATION AND SPEED CONTROL OF A SLIP ENERGY RECOVERY SYSTEM
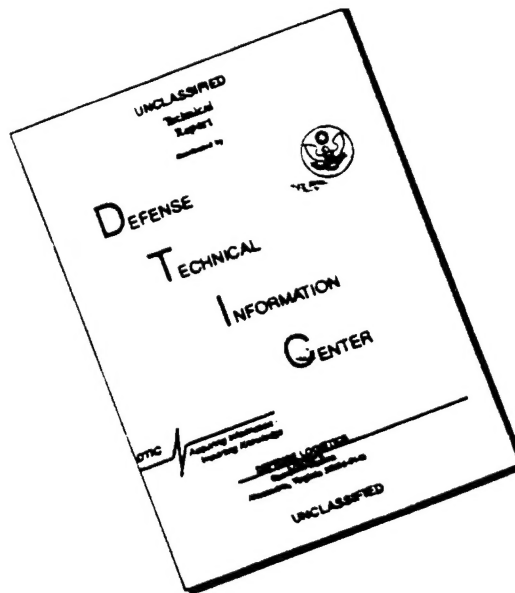
by

Brian S. Tait

December 1995

Thesis Advisor: John G. Ciezki

Approved for public release; distribution is unlimited.

19960401 021

DISCLAIMER NOTICE

THIS DOCUMENT IS BEST QUALITY AVAILABLE. THE COPY FURNISHED TO DTIC CONTAINED A SIGNIFICANT NUMBER OF PAGES WHICH DO NOT REPRODUCE LEGIBLY.

REPORT DOCUMENTATION PAGE		Form Approved OMB No. 0704-0188

Public reporting burden for this collection of information is estimated to average 1 hour per response, including the time for reviewing instruction, searching existing data sources, gathering and maintaining the data needed, and completing and reviewing the collection of information. Send comments regarding this burden estimate or any other aspect of this collection of information, including suggestions for reducing this burden, to Washington Headquarters Services, Directorate for Information Operations and Reports, 1215 Jefferson Davis Highway, Suite 1204, Arlington, VA 22202-4302, and to the Office of Management and Budget, Paperwork Reduction Project (0704-0188) Washington DC 20503.

1. AGENCY USE ONLY *(Leave blank)*	2. REPORT DATE December 1995	3. REPORT TYPE AND DATES COVERED Master's Thesis	
4. TITLE AND SUBTITLE ANALYSIS OF HARDWARE IMPLEMENTATION AND SPEED CONTROL OF A SLIP ENERGY RECOVERY SYSTEM		5. FUNDING NUMBERS	
6. AUTHOR(S) Brian S. Tait			
7. PERFORMING ORGANIZATION NAME(S) AND ADDRESS(ES) Naval Postgraduate School Monterey CA 93943-5000		8. PERFORMING ORGANIZATION REPORT NUMBER	
9. SPONSORING/MONITORING AGENCY NAME(S) AND ADDRESS(ES)		10. SPONSORING/MONITORING AGENCY REPORT NUMBER	
11. SUPPLEMENTARY NOTES The views expressed in this thesis are those of the author and do not reflect the official policy or position of the Department of Defense or the U.S. Government.			
12a. DISTRIBUTION/AVAILABILITY STATEMENT Approved for public release; distribution is unlimited.		12b. DISTRIBUTION CODE	

13. ABSTRACT *(maximum 200 words)*

This thesis involves the construction and testing of a Slip Energy Recovery System (SERS). The principle component of the SERS is a wound rotor induction machine which allows for extraction of slip power from the rotor which in turn provides a means of speed control. Induction machines normally operate at a constant speed, but SERS offers a method of speed control which increases efficiency by returning the slip power back to the system.

In this research effort, various tests required to analyze speed range, signal waveforms and power flow were conducted. Additionally, an analog and a microprocessor-based control scheme were implemented for speed control. A number of studies are presented to validate and contrast the proposed circuits.

The system data collected during validation studies are compared against the theoretical operation of the SERS. After construction, alternative topologies are investigated in order to assess the configuration that provides an optimal speed range. A baseline was established and it is shown that the location of the transformer in the SERS has a significant influence on the speed range.

Results from further testing of the baseline configuration revealed that in regards to waveforms and power flow, the system responded as expected.

4. SUBJECT TERMS induction machine, slip energy recovery, Dspace control			15. NUMBER OF PAGES 118
			16. PRICE CODE

17. SECURITY CLASSIFICATION OF REPORT Unclassified	18. SECURITY CLASSIFICATION OF THIS PAGE Unclassified	19. SECURITY CLASSIFICATION OF ABSTRACT Unclassified	20. LIMITATION OF ABSTRACT UL

ANALYSIS OF HARDWARE IMPLEMENTATION AND SPEED CONTROL OF A SLIP ENERGY RECOVERY SYSTEM

Brian S. Tait
Lieutenant, United States Navy
B.S., United States Naval Academy, 1989

Submitted in partial fulfillment
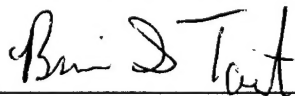of the requirements for the degree of

MASTER OF SCIENCE IN ELECTRICAL ENGINEERING
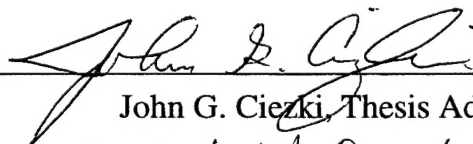
from the

NAVAL POSTGRADUATE SCHOOL
December 1995
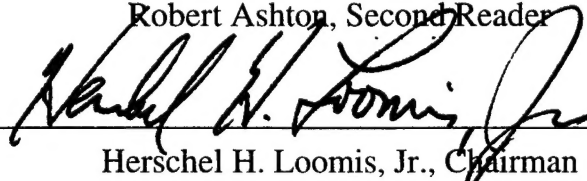
Author: _____
Brian S. Tait

Approved by: _____
John G. Ciezki, Thesis Advisor

_____
Robert Ashton, Second Reader

_____
Herschel H. Loomis, Jr., Chairman
Department of Electrical and Computer Engineering

iii

ABSTRACT

This thesis involves the construction and testing of a Slip Energy Recovery System (SERS). The principle component of the SERS is a wound rotor induction machine which allows for extraction of slip power from the rotor which in turn provides a means of speed control. Induction machines normally operate at a constant speed, but SERS offers a method of speed control which increases efficiency by returning the slip power back to the system.

In this research effort, various tests required to analyze speed range, signal waveforms and power flow were conducted. Additionally, an analog and a microprocessor-based control scheme were implemented for speed control. A number of studies are presented to validate and contrast the proposed circuits.

The system data collected during validation studies are compared against the theoretical operation of the SERS. After construction, alternative topologies are investigated in order to assess the configuration that provides an optimal speed range. A baseline was established and it is shown that the location of the transformer in the SERS has a significant influence on the speed range.

Results from further testing of the baseline configuration revealed that in regards to waveforms and power flow, the system responded as expected.

TABLE OF CONTENTS

I. INTRODUCTION

The induction motor is widely used in industry and in Department of Defense applications as either a constant speed or variable speed device. In recent years, applications for variable speed induction motors have increased. Changing the speed of an induction motor is achieved in two ways: by changing the synchronous speed of the rotating magnetomotive force (mmf) of the stator or by changing the slip.

The first way to implement speed control is to change the mmf_s which involves changing the number of poles of the machine or varying the input line frequency. The second way to implement speed control is to change the slip which involves varying the line voltage input or the rotor resistance. An indirect method of varying rotor resistance is called electromagnetic force (emf) slip injection and the slip energy recovery system (SERS) falls under this category. A SERS offers an indirect way to control rotor voltage. Thus, slip and rotor speed is controlled. This research effort focuses on the development and analysis of a SERS and the implementation of two speed control approaches.

The SERS requires a double-fed wound rotor induction machine. Access to the windings in the rotor is essential to extract the slip power from the rotor. Also required are a transformer, diode bridge rectifier, inductor and thyristor inverter bridge. These components work in conjunction to form the SERS.

The main advantage of the SERS is the lower rated power electronics in the rotor control scheme as compared to a similar stator voltage control scheme. An additional advantage is that rotor slip power is returned to the system and efficiency is improved.

Common applications of the SERS include fan and pump drive systems where the speed control range is narrow and the torque requirements are high (Stemmler, 1994).

The goals of this thesis include:

1. building and validating the operation of a SERS using equipment common to the Power Systems Laboratory,
2. investigating alternative topologies for range of speed control,
3. identifying power flow and efficiency for various operating conditions,
4. developing an analog control for automatically changing rotor speed, and
5. implementing an equivalent digital control using the dSPACE development tools and microprocessor chip (dSPACE, 1993).

Previous research efforts into the SERS include the application of fuzzy logic techniques to improve the performance of a SERS (Borges da Silva, et al. 1992), the use of a step-down chopper control scheme (Refoufi, et al. 1993), the control of power factor (Smith, et al. 1990), the analysis of start-up transients (Akpinar, et al. 1992) and transfer functions schemes (Miles, et al. 1979).

This thesis is organized in the following manner: A system overview is offered in Chapter II. In Chapter III, component and systems equations are developed. Induction machine equations are outlined in Chapter IV. In Chapter V, preliminary hardware schemes are investigated prior to full SERS implementation. Also, in Chapter V, alternative topologies are compared for determining the configuration that yields the optimum range of rotor speeds. Waveforms and power flow throughout the system are discussed in Chapter VI. Chapter VII contains information concerning the analysis and comparison of the two types of controllers implemented, analog and dSPACE. Detailed information on the operation of dSPACE is found in Chapter VIII. Conclusions as well as future research avenues are detailed in Chapter IX.

II. SLIP ENERGY RECOVERY SYSTEM

A. INTRODUCTION

The slip energy recovery system (SERS) is designed to harness the slip power that is normally dissipated on the rotor of a wound-rotor induction machine. The SERS consists of a wound-rotor induction motor, a diode rectifier connected to the rotor windings via slip rings, a direct current (dc) link, a phase-controlled fixed-frequency inverter and frequently a transformer interconnecting the inverter bridge to the stator alternating current (ac) supply.

B. SYSTEM OVERVIEW

In this chapter the individual components of a SERS, illustrated in Figure 2.1, are described, and their functions in the circuit are explained. Speed control is typically achieved in induction machines by either controlling the stator voltages or by adjusting the rotor resistances. In the first case, stator voltage control, the converter must be rated for the full rated voltage of the machine. Since the cost of a converter is proportional to the power rating, the converter in a large horsepower electric drive may represent a large portion of the overall cost. In the latter case, rotor resistance control, the efficiency of the drive is significantly reduced as larger values of resistance are employed on the rotor.

Considering the limitations of these two options for speed control, an alternative method is offered by the SERS. Through control of the firing angle of the inverter, the rotor back emf voltages are automatically adjusted. This allows for control of the slip

power which is transmitted across the air gap. Instead of wasting this power in external

resistors, the SERS routes the slip power back to the input source.
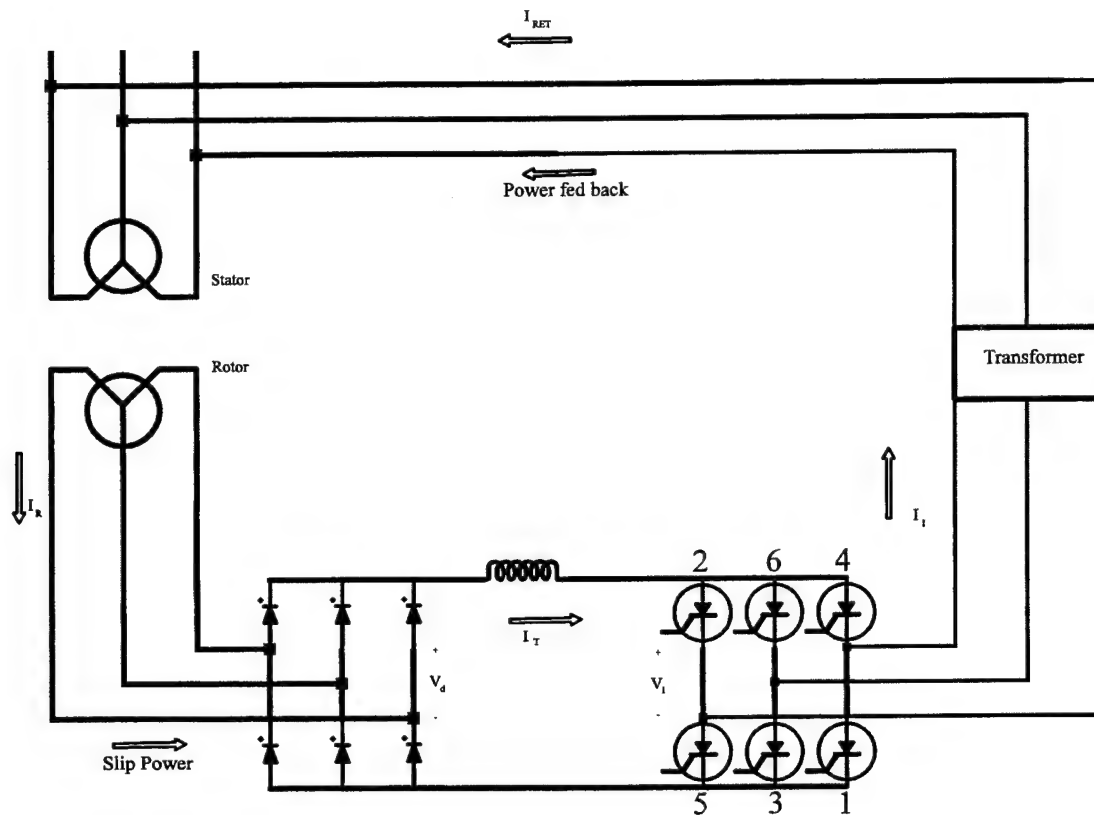
Figure 2.1 Slip Energy Recovery System

In a steady-state condition, the voltage on the dc-side of the rectifier must be

balanced by the voltage on the dc-side of the inverter. This condition must hold in order

for there to be zero voltage across the inductor and no change in the inductor current.

The large inductance in the dc link helps keep the link current constant. By controlling

the firing angle of the inverter, the dc-side inverter voltage is changed, and subsequently,

the rectifier dc voltage is automatically adjusted. The rotor back emf voltages are

proportional to the dc-side rectifier voltage. The amplitudes of the rotor voltages are

large at zero speed (start up) and get smaller as synchronous speed is approached. Thus, speed control is achieved by directly influencing the amplitude of rotor voltages. If the range of speed control is kept between 70-100 % of synchronous speed, then the associated rotor voltages are relatively low. As a consequence, the ratings on the converters will be smaller than drives employing stator voltage control. For large horsepower drives, this translates into a less expensive power converter and a less expensive drive.

The SERS is commonly used in variable speed pump and fan applications where the range of speed control is narrow and adequate braking is provided by the medium used. It will be shown that regenerative braking is not normally available in a SERS. Other typical uses of the SERS include large horsepower applications where the gains in efficiency provide significant economic return.

C. SYSTEM COMPONENTS

In this section, the following components are discussed in the following order: Wound-Rotor Induction Motor, Diode Bridge, dc Link, Three-Phase Inverter, Firing Angle Control, and Transformer.

1. Wound-Rotor Induction Motor

The induction machine is commonly used in industry to convert electrical power into mechanical work. The SERS employs a wound-rotor type induction machine vice a squirrel-cage type induction machine due to the required accessibility of the rotor windings. Wound-rotor type induction machines have access to the rotor windings via slip rings facilitating the injection of voltages and the recovery of slip power. The rotor

windings of squirrel-cage induction machines are made of cast iron and are simple and inexpensive to build, but these windings cannot be made accessible to the outside environment. Additionally, the induction motor used in this research effort was constructed so that the rotor winding connections are conveniently located on the front faceplate of the machine panel and are easily connected to the rest of the SERS.

The principle by which the induction motor operates is explained as follows. At no load, the rotor runs at synchronous speed, and no voltages are induced in the rotor. When a load is applied, the rotor slows so that there is a relative difference in speed (slip) between the stator magnetomotive force and the rotor windings. Voltages are induced in the rotor circuits causing currents to flow, and a rotor mmf is produced. The interaction between this rotor mmf and the stator mmf results in an electromagnetic torque which balances the applied load torque.

2. Diode Bridge

The purpose of the diode bridge is to act as an uncontrolled 3-phase rectifier. The rotor voltages are converted from ac rotor voltages to dc voltage. The voltage on the dc-side of the rectifier is indirectly controlled by varying the firing angle of the inverter. By virtue of the fact that the inductor current in the dc link is constant in the steady-state, the rectifier dc-side voltage is forced to track the inverter dc-side voltage. By controlling the inverter dc voltage via the firing angle, the dc voltage across the rectifier is also controlled.

3. DC Link

The dc link is comprised of a filter inductor. The purposes of the filter inductor are to maintain constant link current and to minimize current ripple delivered to the inverter. Since the link inductor is typically very large, a significant resistance is also associated with the coil. As a result, it is generally required to model the link by an inductor in series with a resistor. In the steady state, the voltage drop across the resistance leads to the dc-side inverter voltage being slightly less than the dc-side rectifier voltage.

4. Three-Phase Inverter

Connected between the dc link and the stator line is the 3-phase inverter which consists of three pairs of thyristors and the associated snubber circuitry. The inverter converts the dc link current into ac current which is then delivered to the ac mains. The inverter is line-commutated by the ac source voltages. The dc-side voltage of the inverter can be controlled by delaying the gating signals to the thyristors from the points of natural commutation. It will be shown later that by changing the firing angle, the average voltage across the thyristor bridge will change, and subsequently, the voltage across the diode bridge will change which causes the rotor injection voltage to change. Finally, since the rotor voltage amplitude is proportional to the difference in synchronous speed and rotor speed, the speed of the motor will change.

5. Firing Angle Control

In the laboratory implementation of the SERS for this research effort, the power thyristors are gated by electronic pulses (0-5 Volt dc) from the thyristor firing control

unit. Physically, an electrical cable containing nine signal wires connects the firing unit to the thyristor module which contains six thyristors with associated snubber circuitry. Signals that are transmitted include: six thyristor gate signals, one synchronization signal, and two common signals. Referring to Fig 2.1, the thyristors are labeled in the order of conduction (gating) from 1 to 6.

The firing of each thyristor is critical. Each thyristor is fired in coordination with the synchronizing input of its respective phase. Two synchronizing inputs from the source are connected to the thyristor control unit where the gating signals are originated. These inputs provide the coordination needed to ensure properly timed firing of each thyristor. For proper operation, the thyristor control unit should have $C\phi$ and $B\phi$ source voltages connected to synchronizing inputs one and two, respectively, both angle control buttons should be in the out position, and the gate control mode button should be in the 3ϕ position.

For an individual phase, the time delay relationship between the zero crossing of the synchronizing signal and the gated signal is denoted as t_α. For a 60 Hz source, this time delay relationship can be translated into a degree relationship expressed as

$$\alpha = \frac{t_\alpha}{16.67\,ms}\, 360^\circ \qquad (2.1)$$

where α is the firing angle and t_α is the time delay between the synchronizing zero crossing and thyristor gating pulse. This type of firing or commutation is called line commutation, where the line voltages are used to automatically turn the thyristors off.

Changing the firing angle, α, changes the time in which the respective thyristor fires in relation to the associated line voltage zero crossing. Also as α changes, the average voltage across the thyristor bridge changes. Firing angle or α control is achieved by varying a dc voltage level input on the thyristor control unit panel. Taking the dc level to its maximum value (+10 volts) corresponds to 180 degrees of delay, while the minimum value (-10 volts) corresponds to 0 degrees of delay. This α control signal is sent to internal circuitry in the thyristor control unit where six thyristor pulse signals are synchronized with the line frequency. Then, these accurately timed signals are sent to the thyristor module via one cord as previously mentioned.

Firing angle control allows the user to change the average voltage level across the thyristor bridge by changing the timing relationship between the synchronizing signal zero crossing and the gate signal firing.

In subsequent chapters, it is important to note that equations have been developed with α referenced to the crossover points of the line voltages instead of the zero crossing of the line voltage which is what the thyristor firing control unit uses as a reference. This causes a 60° shift in the relationship of the alphas which is expressed as

$$\alpha_o + 60^o = \alpha \qquad (2.2)$$

where α_0 is the alpha for the equations and α is the value displayed on the thyristor firing control unit.

In Chapter III, specific equations are developed for the SERS used in this research effort using α_0. In Chapters V - VII, studies are conducted on the SERS and referenced to the α displayed on the thyristor firing control unit.

9

6. Transformer

As shown in Figure 2.1, a transformer is usually located between the inverter and the ac mains. In choosing the optimum value of the turns ratio, the power factor and the operational speed range of the SERS are maximized. A detailed description of this optimization is provided in subsequent chapters.

In this research effort, the transformer was placed between the rotor and the diode bridge with a 1:2 turns ratio as shown in Figure 2.2. The reason for this location and ratio is to boost the rotor voltage output in order to ensure diode commutation. This rationale is explained further in subsequent chapters. The location and turns ratio of the transformer significantly impacts the performance of the system with regard to the power factor and range of speed control.

D. BASIC SPEED CONTROL USING THE ROTOR CIRCUITRY

In this section, the following topics are discussed: Rotor Resistance Control, Diode Bridge with Variable Load Resistance, and the Integrated System.

1. Rotor Resistance Control

In the initial phase of developing the SERS, speed control of the induction machine was investigated by varying the resistance of the rotor as depicted in Figure 2.3. By increasing (decreasing) the resistance of the rotor, the speed of the motor is decreased (increased). Thus, for wound-rotor induction machines, changing the resistance on the rotor is one way to change the speed of the machine. The attractive feature of this means of speed control is that the additional rotor resistance can be placed away from the machine, therefore, not affecting the cooling requirements of the machine.

10
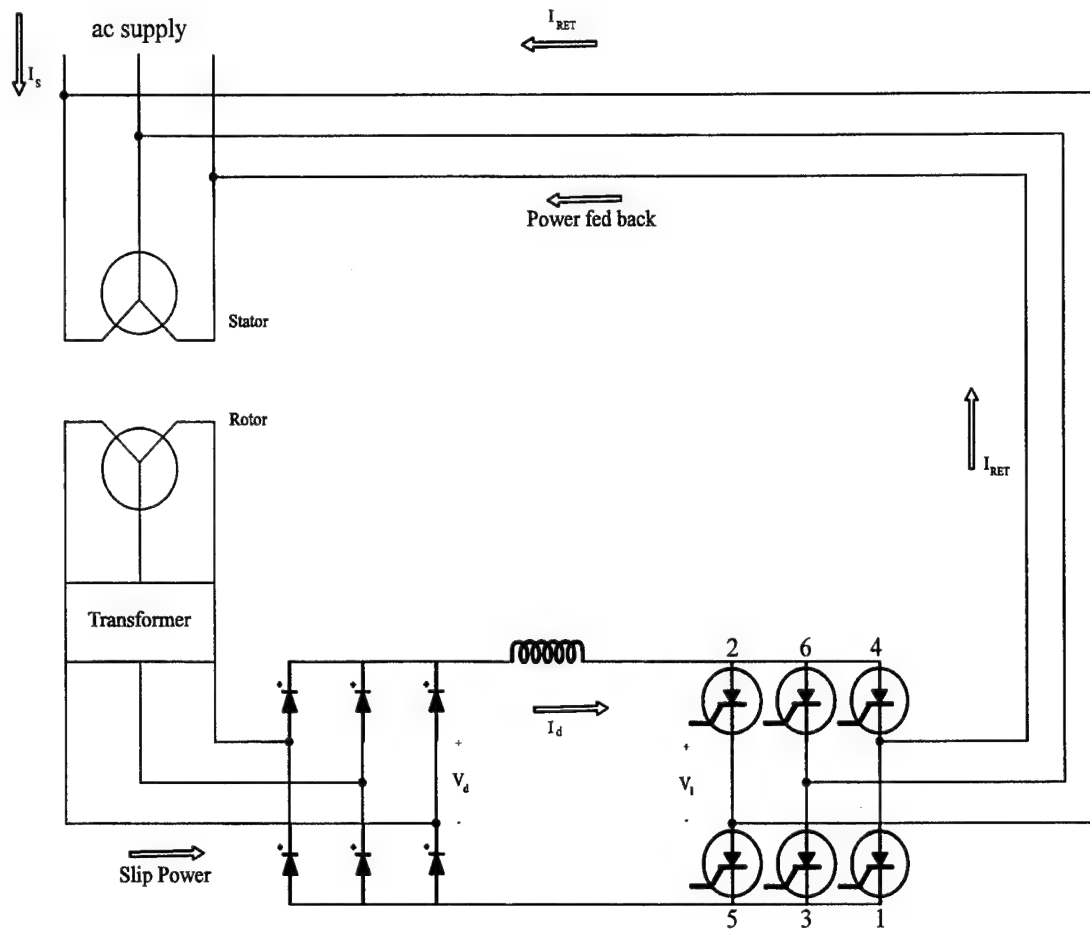
Figure 2.2 Modified SERS

This method of speed control is not very efficient and thus is used primarily in applications where simplicity is more important than efficiency.
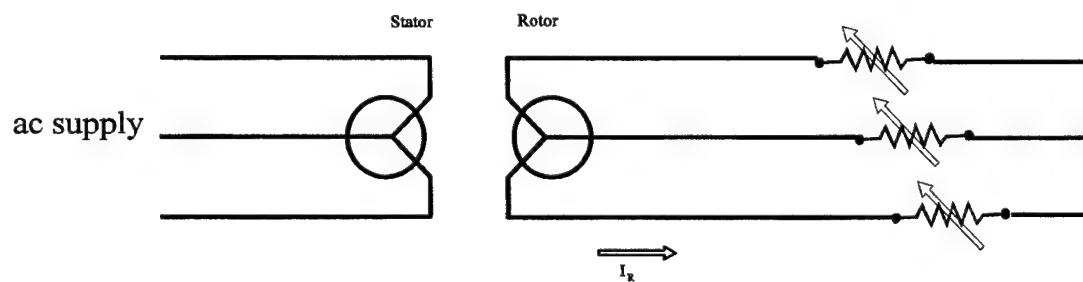
Figure 2.3 Variable Rotor Resistance Scheme

11

2. Diode Bridge with Variable Load Resistance

Before implementing the entire SERS, a diode bridge with variable load resistance scheme was configured as shown in Figure 2.4. As the load resistance is increased for a given load torque, more slip power is extracted from the rotor and the speed of the motor decreases. Conversely, as the load resistance is decreased for a given load torque, the equivalent rotor resistance is decreased, less power is extracted from the rotor, and the speed of the motor increases. In this scheme, speed control is achieved, but the approach is inherently inefficient due to the waste of slip power in the external resistance. Unlike the variable load resistance schemes, the SERS will improve efficiency while still realizing an appropriate range of speed control.
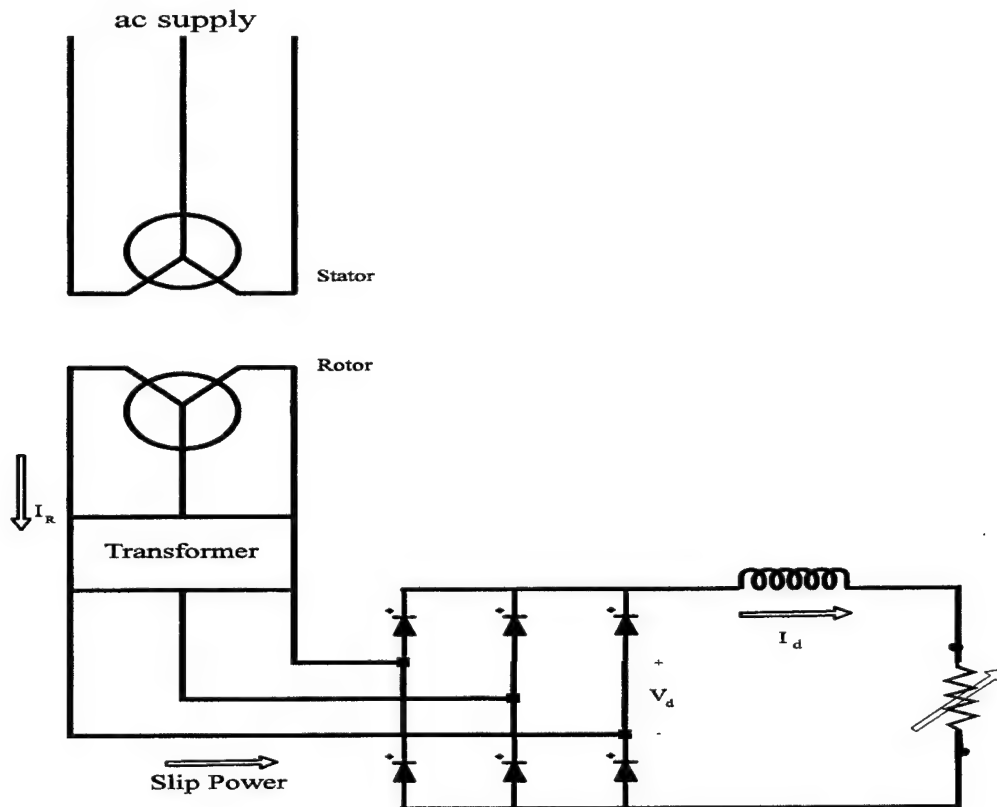
Figure 2.4 Diode Bridge with Variable Resistance

12

3. Integrated System

The SERS investigated in detail in this research effort is illustrated in Figure 2.2. The efficiency of a wound-rotor induction machine drive is improved by extracting slip power off of the rotor, rectifying it, inverting it and then, sending it back to the system. As a result, the efficiency of the overall system is improved.

Speed control is achieved by controlling the counter-emf injection into the rotor. This process starts by varying the firing angle of the thyristors. At $\alpha = 180^\circ$, the average value of V_I is a maximum, and as α decreases, the average value of V_I decreases correspondingly. The average value of V_I can be viewed as an injected emf opposing the rectified rotor voltage. In this example, as V_I decreases, the injection emf opposing the rectified rotor voltage decreases, current begins to flow in the link implying current flows in the rotor windings. With rotor current flowing, a torque is produced and the machine accelerates. As the motor speed increases, the relative speed between the stator mmf and the rotor decreases, and the rotor induced emf decreases. Steady state is achieved when the decrease in dc-side rectifier voltage matches the decrease in the dc-side inverter voltage and the appropriate link current flows to balance the applied load torque. As α increases, the opposite occurs: the average value of V_I increases, the link current decreases, rotor currents decrease, a smaller torque is produced, and motor speed decreases. Thus, speed control is achieved by adjusting α.

E. CONCLUSION

The SERS is designed to increase the efficiency of a wound-rotor induction machine drive and to implement speed control by placing the power electronics on the

rotor-side of the machine. It improves efficiency by capturing the slip power that is normally dissipated on the rotor and redirecting the slip power to the stator and source. All this is accomplished through a diode bridge, dc link, inverter and transformer scheme. In addition for a narrow range of speed control near synchronous speed, the SERS topology facilitates the application of a converter with a smaller power rating than that for an equivalent stator voltage control topology.

III. SYSTEM EQUATIONS

A. INTRODUCTION

In this chapter the equations required to model the individual components of the SERS are developed, and an analysis of how the interconnected system operates is presented.

B. COMPONENT EQUATIONS

1. Induction Machine

The induction machine used in the SERS is a wound rotor, 4 pole, 3-phase, wye-connected machine. It is reasonable to assume that the stator windings are symmetrically wound 120° apart with each having N_s equivalent turns and a resistance of r_s. The parameter values for the particular machine used are detailed in Chapter IV. Similarly, the rotor windings are assumed to be symmetrically wound 120° apart with each having N_r equivalent turns and a resistance of r_r. Figure 3.1 illustrates the assumed winding configuration.

The induction machine voltage equations may be expressed in the matrix form:

$$\vec{v}_{abcs} = r_s \vec{i}_{abcs} + p \vec{\lambda}_{abcs} \tag{3.1}$$

$$\vec{v}_{abcr} = r_r \vec{i}_{abcr} + p \vec{\lambda}_{abcr} \tag{3.2}$$

where "p" is the Heaviside operator, "v" denotes voltage, "i" denotes current, and "λ" denotes flux linkage. The vector notation is shorthand for

$$\left(\vec{f}_{abcs} \right)^T = \left[f_{as}\, f_{bs}\, f_{cs} \right] \tag{3.3}$$

15

$$\left(\vec{f}_{abcr}\right)^T = \left[f_{ar}\ f_{br}\ f_{cr}\right] \tag{3.4}$$

where "f" may be "v", "i", or "λ".
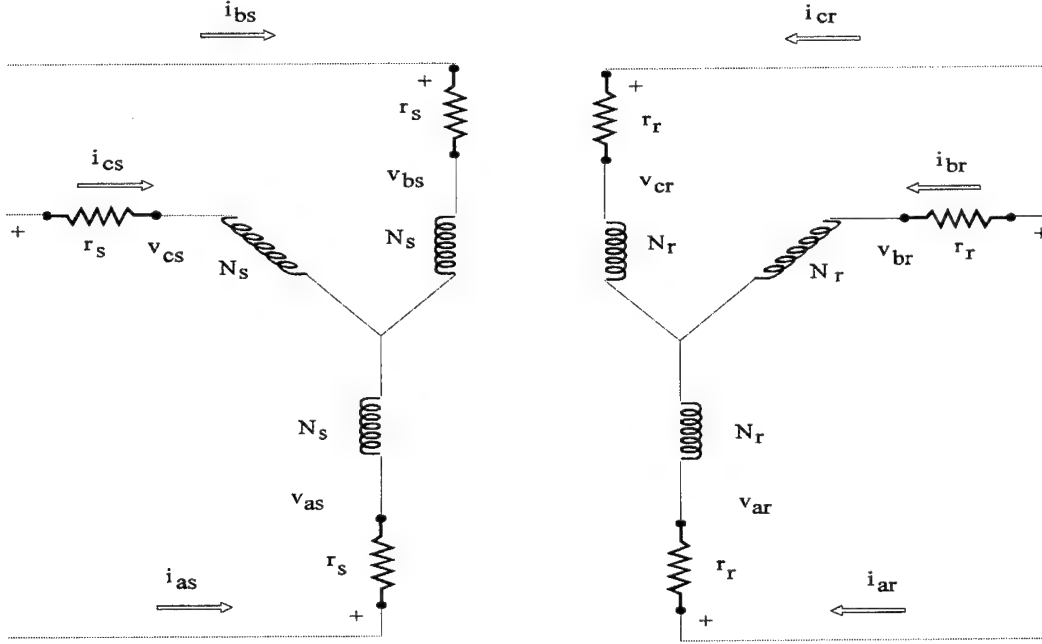
Figure 3.1 Induction Machine Winding Configuration

The s and r subscripts denote variables and parameters associated with the stator and rotor circuits, respectively. The r_s and r_r components are equal element diagonal resistance matrices for the stator and rotor.

Taking into consideration the turns ratio, N_s/N_r, the rotor-side voltage, current and flux linkage can be referred to the stator-side by the following change of variables:

$$i'_{abcr} = \frac{N_r}{N_s} i_{abcr} \tag{3.5}$$

$$v'_{abcr} = \frac{N_s}{N_r} v_{abcr} \tag{3.6}$$

$$\lambda'_{abcr} = \frac{N_s}{N_r} \lambda_{abcr} \tag{3.7}$$

16

In a magnetically linear system and assuming that slot harmonics may be ignored, the flux linkages referred to the stator side can then be expressed as

$$
\begin{bmatrix} \lambda_{abcs} \\ \lambda'_{abcr} \end{bmatrix} = \begin{bmatrix} L_s & L'_{sr} \\ \left(L'_{sr}\right)^T & L'_r \end{bmatrix} \begin{bmatrix} i_{abcs} \\ i'_{abcr} \end{bmatrix}
\tag{3.8}
$$

where the submatrices are given by

$$
L_s = \begin{bmatrix} \left(L_{ls} + L_{ms}\right) & -\frac{1}{2} L_{ms} & -\frac{1}{2} L_{ms} \\ -\frac{1}{2} L_{ms} & \left(L_{ls} + L_{ms}\right) & -\frac{1}{2} L_{ms} \\ -\frac{1}{2} L_{ms} & -\frac{1}{2} L_{ms} & \left(L_{ls} + L_{ms}\right) \end{bmatrix}
\tag{3.9}
$$

$$
L'_r = \begin{bmatrix} \left(L'_{lr} + L_{ms}\right) & -\frac{1}{2} L_{ms} & -\frac{1}{2} L_{ms} \\ -\frac{1}{2} L_{ms} & \left(L'_{lr} + L_{ms}\right) & -\frac{1}{2} L_{ms} \\ -\frac{1}{2} L_{ms} & -\frac{1}{2} L_{ms} & \left(L'_{lr} + L_{ms}\right) \end{bmatrix}
\tag{3.10}
$$

$$
L_{sr} = L_{sr} \begin{bmatrix} \cos \theta_r & \cos\left(\theta_r + \frac{2\pi}{3}\right) & \cos\left(\theta_r - \frac{2\pi}{3}\right) \\ \cos\left(\theta_r - \frac{2\pi}{3}\right) & \cos \theta_r & \cos\left(\theta_r + \frac{2\pi}{3}\right) \\ \cos\left(\theta_r + \frac{2\pi}{3}\right) & \cos\left(\theta_r - \frac{2\pi}{3}\right) & \cos \theta_r \end{bmatrix}
\tag{3.11}
$$

The angle θ_r is the rotor electrical angle which is related to the actual rotor position by the number of pole pairs.

The referred rotor and stator leakage inductances are given by L'_{lr} and L_{ls}. The magnetizing inductance associated with the stator is given by L_{ms}. Also, it can be shown that $L_{ms} = aL_{sr}$ and $L'_{sr} = aL_{sr}$ where $a = N_s/N_r$. The magnitude of the stator to rotor mutual inductance is given by L_{sr}.

17

The voltage equations with the rotor variables referred to the stator-side can be expressed as

$$
\begin{bmatrix} v_{abcs} \\ v'_{abcr} \end{bmatrix} = \begin{bmatrix} r_s + pL_s & pL'_{sr} \\ p\left(L'_{sr}\right)^T & r'_r + pL'_r \end{bmatrix} \begin{bmatrix} i_{abcs} \\ i'_{abcr} \end{bmatrix}
\tag{3.12}
$$

where

$$
r'_r = \left(\frac{N_s}{N_r} \right)^2 r_r
\tag{3.13}
$$

An equation for the electromagnetic torque of a P-pole machine is derived in Krause et al. (1986) and is expressed as

$$
T_e = \left(\frac{P}{2} \right) (i_{abcs})^T \frac{\partial}{\partial \theta_r} \left[L'_{sr} \right] i'_{abcr}
\tag{3.14}
$$

The torque and the speed are related by

$$
T_e = J \left(\frac{2}{P} \right) p\, \omega_r + T_L
\tag{3.15}
$$

where J is the inertia of the motor and load, T_L is the applied load torque, and P is the number of magnetic poles for which the machine is wound.

2. Average Value Model of Diode Rectifier

A diode bridge is connected to the dc link which auctioneers slip power back to the ac source and stator through the fixed-frequency inverter. In this section, an average value model is presented for the diode bridge in the SERS.

Basic assumptions in the analysis of the SERS include the following:

1. commutation in the rectifier is ignored,
2. link inductor current is dc,

18

3. rotor phase current is assumed to have a 120° current pulse shape where steady-state torque is produced by the fundamental component only,
4. losses in the rectifier are ignored,
5. the transformer is assumed to be ideal,
6. commutation overlap in the inverter is neglected.

For a six-pulse rectifier the average dc-side voltage can be expressed as

$$V_d = \frac{3\sqrt{3}}{\pi} V_m \cos \alpha \qquad (3.16)$$

where V_m is the peak ac rotor phase voltage (Dubey, 1989).

With the previously mentioned assumptions and neglecting the stator and rotor leakage impedance drops, V_d can be expressed with $\alpha = 0$ as

$$V_d = \frac{3\sqrt{6}}{\pi} \frac{sV}{a_{T1}} \qquad (3.17)$$

when

$$V_m = \frac{sV\sqrt{2}}{a_{T1}} \qquad (3.18)$$

where V is the stator root mean square (rms) phase voltage, s is the slip, and a_{T1} is the stator to rotor turns ratio.

3. DC Link Equations

In the dc link, the inductor is considered lossless; therefore, any series resistance is ignored. The inductor serves the purposes of maintaining a continuous current condition and minimizing current ripple. The dc link connects the rectified rotor quantities to the inverter which unfolds the dc quantities to produce ac quantities at line frequency. Previously, an equation for the average value of the dc-side diode bridge

voltage was shown. With the assumption of an ideal inductor with dc link current, the steady-state voltage drop across the inductor must be zero so that

$$V_d + V_I = 0 \tag{3.19}$$

This equation is important because it shows that in the steady-state V_d which depends on the motor slip must balance out V_I which will be shown to depend on the inverter firing angle.

4. Average Value Model of Thyristor Inverter

The average value representation of the inverter voltage can be expressed as

$$V_I = \frac{3\sqrt{6}}{\pi} V \cos \alpha_o \tag{3.20}$$

where V is the stator rms phase voltage and α_o is the inverter firing delay angle. The development of Equation 3.20 assumes instantaneous thyristor commutation and continuous current conduction. The angle α_o is referenced from the intersection point of the various line-to-line source voltages. These intersection points are termed the natural points of commutation.

Upon incorporating the effect of a transformer between the source and the inverter, the inverter average voltage equation becomes

$$V_I = \frac{3\sqrt{6}}{\pi} \frac{V}{a_{T2}} \cos \alpha \tag{3.21}$$

where a_{T2} is the turns ratio of the transformer (ac supply side/inverter ac-side). In this research effort, a_{T2} is one since there is no transformer between the inverter and the ac mains. It was relocated between the rotor windings and diode bridge. This relocation of

20

the transformer is manifested by effectively changing the stator/rotor turns ratio of the machine, a_{T1}.

C. INTEGRATED SYSTEM EQUATIONS

1. Steady-State Analysis

In order to establish the operation of the integrated SERS, a steady-state analysis is first performed. If the previous assumptions are considered together with the relocation of the transformer, the average voltage output of the diode bridge is now expressed as

$$V_d = \frac{3\sqrt{6}}{\pi} sV \tag{3.22}$$

where $V_m = sV$ because of the placement of the transformer between the rotor and the diode bridge renders $a_{T1}=1$. The stator to rotor turns ratio is 2:1 while the transformer turns ratio is 1:2. From Equation 3.21, the average counter emf of the inverter reduces to

$$V_I = \frac{3\sqrt{6}}{\pi} V \cos \alpha_o \tag{3.23}$$

given that there is no transformer between the inverter and the ac mains, implying that $a_{T2}=1$.

Given at no load that $T_e=0$, $I_d=0$ and $V_d+V_I=0$, Equations 3.22 and 3.21 can be combined to give

$$2.34 sV + 2.34 V \cos \alpha_o = 0 \tag{3.24}$$

Solving for the slip, s, yields

$$s = -\cos \alpha_o \tag{3.25}$$

21

Slip is defined as

$$s = \frac{\omega_e - \frac{P}{2}\omega_{rm}}{\omega_e} \qquad (3.26)$$

where P is the number of poles for the induction machine and ω_{rm} is the actual speed of
the rotor. For the induction machine used in the SERS where P=4, Equation 3.26
becomes

$$s = \frac{\omega_e - 2(\omega_{rm})}{\omega_e} \qquad (3.27)$$

Upon substituting Equation 3.27 into Equation 3.25, ω_{rm} can be expressed as

$$\omega_{rm} = \frac{1}{2}\omega_e\left(1 + \cos\alpha_o\right) \qquad (3.28)$$

Equation 3.25 illustrates that by changing α_o, the slip changes and thus, the steady-state
speed is adjusted. The speed control can range from near synchronous speed to standstill
when the range of α_o is 90-180°, respectively. The lower range is determined by the
inability of the diode bridge to have a negative voltage drop. When α_o decreases to 90°,
the voltage drop across the diode bridge voltage is zero and alpha cannot go any lower.
The upper range is defined by limits on the natural commutation of the inverter.
Equation 3.28 illustrates that the rotor speed is determined by α_o and is independent of
load torque. This fact holds since Equation 3.28 is valid as long as the dc link current is
constant.

Torque is developed as currents are induced in the rotor windings. As the
induction motor is loaded, the rotor speed of the motor is decreased slightly which causes
a slight increase in slip. An increase in slip causes an increase in the induced voltages

22

and currents. The higher the value of the rotor current flowing the more torque output produced which matches the load.

With small rotor resistance, the rotor slip power or air gap power is approximately equal to the dc link power which is expressed as

$$s\ P_g\ =\ V_d\ I_d \tag{3.29}$$

where sP_g is the rotor slip power. Given that

$$P_g\ =\ T\ \omega_e \tag{3.30}$$

where T is the electrical torque and upon substituting Equation 3.30 into Equation 3.29, the torque is found to be given by

$$T\ =\ \frac{V_d\ I_d}{s\ \omega_e} \tag{3.31}$$

Furthermore, upon substituting Equation 3.22 into Equation 3.31, the developed torque is given by

$$T\ =\ \frac{3\sqrt{6}}{\pi}\ \frac{V\ I_d}{\omega_e} \tag{3.32}$$

which shows that it is proportional to the dc link current, I_d. The fundamental rms rotor current is related to the dc link current by Dubey (1989) as

$$I_r\ =\ \frac{\sqrt{6}}{\pi}\ I_d \tag{3.33}$$

Therefore, the resulting equation relating torque and fundamental rms rotor current is expressed as

$$T\ =\ \frac{3V\ I_r}{\omega_{rm}} \tag{3.34}$$

23

2. Angle Control

In this section, the effects of changing α_o, the inverter firing angle, are examined. In particular, the dynamics of a speed change are explained.

In the inverter operation, α_o is maintained between 90° and 180°, thus the permissible slip is always positive and extends from 0 to 1. This illustrates that in the subsynchronous region, the motor speed can be controlled by changing the firing angle.

From our assumptions, the rotor current will have a 120° pseudo-rectangular waveform with the fundamental being in phase with the slip frequency rotor phase voltages. For a given operating condition, V_d and V_I must add to give zero. If α_o decreases, V_I decreases. For a given V_d, I_d temporarily increases and more torque is produced than the load requires. Rotor speed increases and rotor voltages decrease. The diode bridge voltage, V_d, decreases until it is balanced with V_I. The link current, I_d, settles out to a value needed to balance the load torque.

3. Power Flow

The main disadvantage of the SERS drive is its inherently low power factor. It can, however, be optimized. In this section, power flow, power factor and optimization are investigated.

In the SERS, reactive power is drawn by the inverter for the given range of α_o. In the operating area α_o=90° to 180°, as α_o decreases the amount of reactive power consumed by the machine increases (Hildebrandt, 1986). The smaller the angle, the smaller the injected emf, the lower the slip and the higher the motor speed.

For a given α_o, the net power of the system, P_{tot}, is given by

24

$$P_{tot} = P_{mot} - P_{inv} \tag{3.35}$$

where P_{mot} is the power absorbed by the motor and P_{inv} is the power returned by the inverter.

The total reactive power, Q_{tot}, can be expressed as

$$Q_{tot} = Q_{mot} + Q_{inv} \tag{3.36}$$

where Q_{mot} and Q_{inv} are reactive powers absorbed by the motor and inverter, respectively.

At low speeds, the system power factor is noticeably low. For a given low speed (higher α_o value), the total power consumed is small compared to the total reactive power absorbed. Thus, at low speeds, the system has a poor power factor. The α_o angle is high which yields less reactive power and delivers more real power but not enough to overcome the undesirable balance between real and reactive powers. For this reason, in order to optimize efficiency, α_o is normally controlled to keep the rotor speed between 70-100% of synchronous speed which implies α_o is normally kept at a lower value.

To achieve the highest system power factor, the maximum firing angle of the inverter should correspond to the lowest possible speed (Hildebrandt, 1986). This is normally achieved by making the transformer turns ratio equal to the maximum slip shown by the relationship

$$\frac{s}{a_{T1}} = -a_{T2} \cos \alpha_o \tag{3.37}$$

where a_{T1} is the stator to rotor turns ratio and a_{T2} is the return line transformer ac mains to inverter-side turns ratio (Hildebrandt, 1986). In this research effort, a_{T1} and a_{T2} are

effectively one, and solving for α_o yields the maximum angle limit, 180°, for optimum system power factor.

D. CONCLUSION

In this chapter, the system component equations were investigated in detail. System integration was developed and it was shown that speed control can be achieved by varying the inverter firing angle. Power factor was considered and shown to be optimal in a narrow speed range with proper stator and transformer turns ratios.

IV. SYSTEM COMPONENTS AND PARAMETERS

A. INTRODUCTION

The equipment used to implement the slip energy recovery system (SERS) is introduced in this chapter. In particular, the parameters of components such as the induction machine and link inductor are identified. This information is key for duplicating studies as well as for developing accurate digital representations. The 3-phase wound rotor induction machine has three windings roughly sinusoidally distributed about the stator and three windings roughly sinusoidally distributed about the rotor. If a balanced set of 3-phase voltages are applied to the stator, a rotating magnetic field is produced which induces voltages and currents in the rotor windings. The rotor voltages and currents also produce a magnetic field which tries to align itself with the rotating field produced by the stator. This is the principle by which torque is produced in the induction machine.

Determining the machine parameters is essential for proper simulation and analysis of the machine. In this chapter, the results of two tests (no-load and locked-rotor) are presented, machine parameters are derived, and a T-equivalent model is developed. Figure 4.1 illustrates the T-equivalent model and the pertinent parameters that are derived using the no-load and locked-rotor tests.

The machine used in this research endeavor is a 4-pole, 1/4 horsepower machine with a rated rms line-to-line voltage of 208 V, a rated rms stator current of 1.3 A, a rated rms rotor current of 2 A, a rated rms rotor phase voltage of 60 V, and a rated speed of

27

1500 rpm. The motor, model number 8231, is manufactured by Lab Volt. The serial

number of the machine used in the Power Systems Laboratory is M057872. Prior to the

no-load test, each stator phase resistance was measured using an ohm meter. The results

are given in Table 4.1. The average stator resistance, 11.8 Ω, was then used in the

calculations required to determine the remaining parameter values. It is well understood

that this value may change due to heating effects in the machine. Also, it is understood

that this method of determining the resistance does not take into account the fact that ac

currents will flow in the windings. Skin effects are considered negligible.
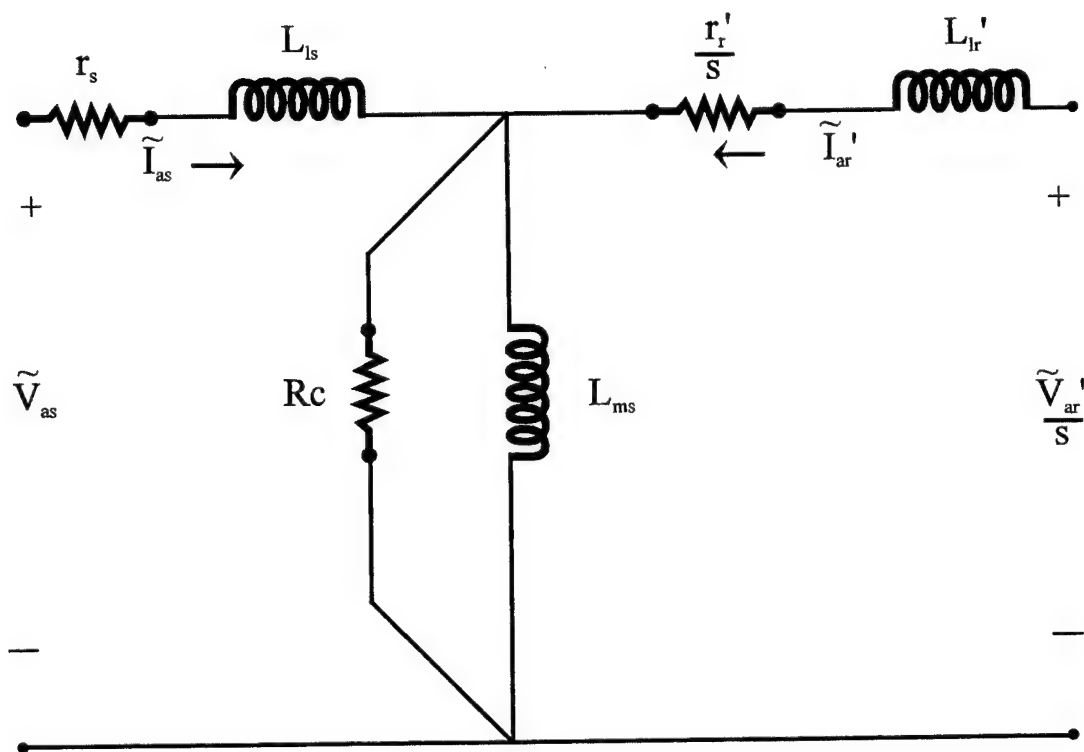
Figure 4.1 T-Equivalent Model

winding	ohms
1-4	11.72
2-5	11.88
3-6	11.80
ave	11.80

Table 4.1 Stator Resistance (r_s) Data

B. NO-LOAD TEST

The first test performed was the no-load test. During this test, the induction machine operates at rated voltage with no load attached to the rotor. Figure 4.2 illustrates the connections required by the particular equipment.
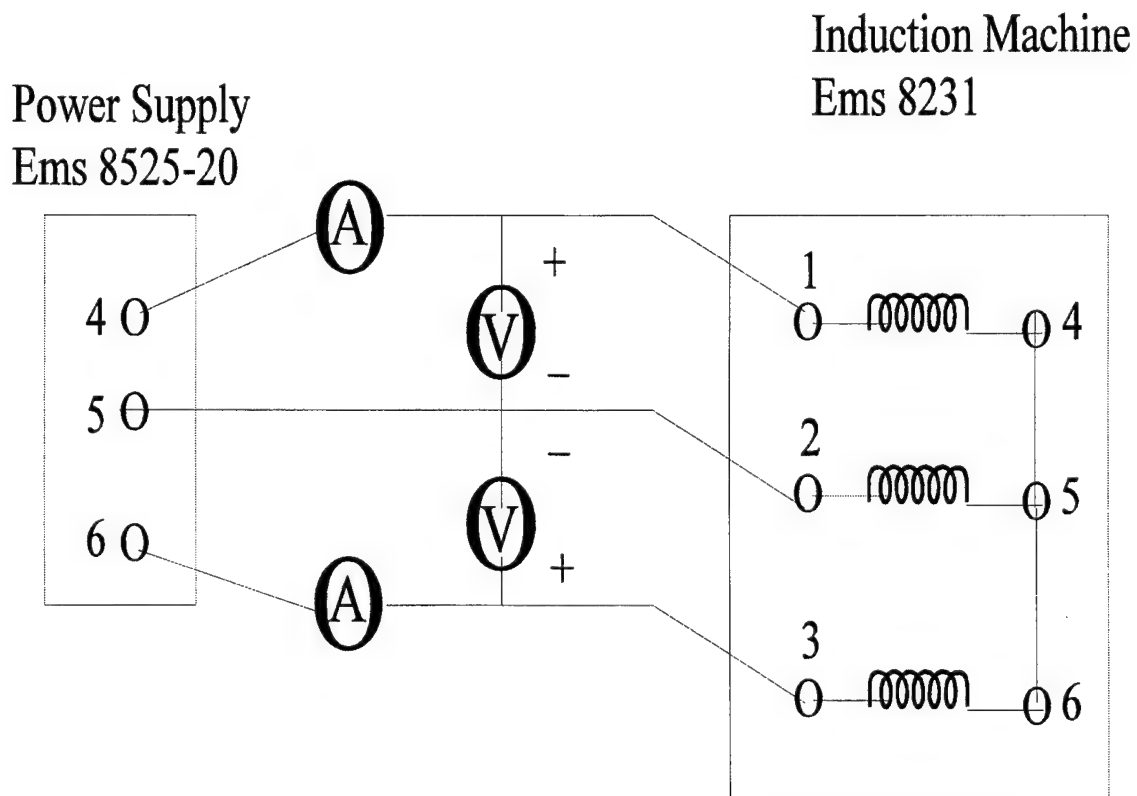

Figure 4.2 No-Load and Locked-Rotor Tests Configuration

During the no-load test, two line-to-line voltages, two phase currents and the real power into the machine are measured. The results are reported in Table 4.2.

$V_{ac} = 204.2$ V	$V_{bc} = 204.9$ V
$i_{as} = .778$ A	$i_{bs} = .781$ A
$P_1 = 102.3$ W	$P_2 = -55.5$ W

Table 4.2 No-Load Data

Also, f = 60 Hz and

$$P_{nL} = P_1 + P_2 = 102.3 - 55.5 = 46.8 \text{ W} \tag{4.1}$$

From the line-to-line voltage, the phase voltage is obtained by

$$\tilde{V}_{ab} = \sqrt{3} \, \tilde{V}_{as} \tag{4.2}$$

During the no-load test, the slip is very small and the rotor branch impedance is large and may be ignored, therefore, the real power into the machine is dissipated in the stator and core loss resistances. The power dissipated in the core loss resistance is equal to the real input power minus the stator copper loss as follows

$$P_{core,nL} = P_{in,nL} - 3\left|\tilde{I}_{as,nL}\right|^2 r_s \tag{4.3}$$

where $\tilde{I}_{as,nL}$ is the no-load phase current.

Once the power dissipated in the core is calculated, it is common to then assume that the voltage across the magnetizing branch is the applied voltage. As a result, the core loss resistance is simply expressed as

$$R_c = \frac{3\left|V_{as,nL}\right|^2}{P_{core,nL}} \tag{4.4}$$

30

The machine at no load is very inductive and the input impedance is given by

$$\frac{\left|\tilde{V}_{as,nL}\right|}{\left|\tilde{I}_{as,nL}\right|} = \sqrt{\left(r_s^2 + \left(x_m + x_{ls}\right)^2\right)} \tag{4.5}$$

From Equation 4.5 the sum of reactances $x_m + x_{ls}$ is found. Using Equation 4.2 and Table 4.2, the phase voltage, V_{as}, is calculated to be 117.89 volts. From Equation 4.3 and Tables 4.1 and 4.2, the power lost in the core is found to be $P_{core,nL}$=25.37 W. Using Equations 4.2, 4.3, and 4.4, R_c is found to be 1643 ohms. Lastly with the data given, the value of $x_m + x_{ls}$ can be determined. Using Equation 4.5, $x_m + x_{ls}$ is calculated to be 151.1 ohms.

C. LOCKED-ROTOR TEST

The locked-rotor test configuration is illustrated in Figure 4.2 with the motor now connected to an electrodynamometer via a timing belt. A maximum load is applied to the machine so that the rotor remains stationary. A reduced line-to-line voltage of approximately 60 V ac is applied to the machine so that roughly rated stator currents flow. Upon energizing the circuit, voltages, currents and powers are quickly measured. The results are given in Table 4.3.

V_{ac} = 67.42 V	V_{bc} = 66.93 V
i_{as} = 1.207 A	i_{bs} = 1.193 A
P_1 = 82.0 W	P_2 = 31.07W

Table 4.3 Locked-Rotor Data

Also, f = 60 Hz and

$$P_{in,lr} = P_1 + P_2 = 82.0 + 31.07 = 113.07 \text{ W} \tag{4.6}$$

During the locked-rotor test, the slip is equal to one. Therefore, the rotor-branch impedance is very small. The comparatively large parallel impedance located in the magnetizing branch may be ignored. Hence, real power is dissipated in the stator and rotor resistances. The following equation applies:

$$r_s + r_r' = \frac{P_{in,lr}}{3\left|\tilde{I}_{as,lr}\right|^2} \tag{4.7}$$

where $\tilde{I}_{as,lr}$ is the locked-rotor phase current.

With r_s=11.8 ohms and using Equations 4.7 and 4.6 with Table 4.3, the referred rotor resistance, r_r', is found to be 14.07 ohms.

With the magnetizing impedance ignored, the input impedance is given by

$$\frac{\left|\tilde{V}_{as,lr}\right|}{\left|\tilde{I}_{as,lr}\right|} = \sqrt{\left((r_s + r_r')^2 + (x_{lr}' + x_{ls})^2\right)} \tag{4.8}$$

Using Equation 4.8, the sum of the leakage reactances, $x_{lr}'+x_{ls}$, is found to be 19.26 Ω. Also, if it is assumed that $x_{lr}'=x_{ls}$ then it follows that $x_{lr}'=x_{ls}$=9.63 Ω. Referring back to the results of the no-load test, x_m+x_{ls}=151.1 Ω, the magnetizing reactance x_m is found to be 141.47 Ω.

D. OTHER MACHINE AND SYSTEM PARAMETERS

The wound rotor induction machine used was a 3-phase, 4-pole machine. The stator to rotor turns ratio is roughly 2:1. The actual manufacturer's data supplied by Arsenault (1995) lists the turns ratio as 516/264. The inertia is listed as 0.0024 kg/m^2 or

32

0.057 lb/ft^2. This information is important and useful in creating an accurate computer model of the induction machine.

Table 4.4 contains pertinent information concerning the other components used in the hardware implementation of the SERS constructed in this research effort.

E. CONCLUSION

Two tests were run and the data were analyzed to derive the parameters needed to characterize the induction machine in the SERS. A few sound assumptions were made to simplify the calculations, and the results appeared reasonable as compared to nominal machine parameters as reported by the manufacturer. A T-equivalent circuit model was derived and the remaining machine parameters were obtained from the manufacturer. The hardware used to implement the remainder of the SERS was identified together with the voltage and current ratings.

Component	Manufacturer	Part #	Value (s)	Voltage Rating	Current Rating
Link Inductor	Lab Volt	8325-10	0.8 H, 4.69 Ω (series)		1.5 A dc
Diode Rectifier	Lab Volt	8842-10		208 V 3 φ	Each Diode 2 A rms
Inverter	Lab Volt	8841-20		208 Vac 1-1	Each Thyristor 2 A rms
Inverter Firing Unit	Lab Volt	9030-30	0-180°	-10 to 10 Vdc	
Firing Unit Power Supply	Lab Volt	8840-00		120 Vac	0.8 A
Transformer	Lab Volt	8348-00	250 VA Limit	208 Vac	1.2 A
Load Dynamometer	Lab Volt	8911	0-27 (lbf-in)	120 Vac	2 A
System Power Supply	Lab Volt	8525-20		0-208 Vac 0-120 Vdc	15 A ac 25 A dc

Table 4.4 SERS Component Parameters

V. PRELIMINARY HARDWARE STUDIES

A. INTRODUCTION

In this chapter, preliminary configurations are studied prior to implementing the

entire SERS. Following these validation studies, the end-to-end SERS is reported on.

Upon implementing the SERS, the effect of changing the location of the transformer is

investigated. In particular, studies are presented with the transformer inserted between

the rotor and diode bridge, between the inverter and source, and with no transformer at

all. An emphasis was placed on the available speed range and current limitations of the

devices.

B. VARYING ROTOR RESISTANCE

During early testing, the system depicted by Figure 5.1 was constructed and

tested. By varying the rotor resistance, the speed of the induction motor is controlled. In

particular, as the rotor resistance is increased, the rotor speed decreases. This is not an

efficient means of controlling the induction motor since the motor efficiency is reduced at

larger values of slip. This reduction in efficiency is manifested in the fact that the

additional slip power is dissipated in the external resistors. The SERS seeks to utilize this

slip power by auctioneering it back around to the stator and source.

C. DIODE BRIDGE WITH A VARYING LOAD RESISTANCE

The next step in the process of building the SERS was to incorporate a diode

bridge and inductor between the rotor and variable load resistor. The diode bridge

rectifies the voltage and then passes this voltage to the dc link. The system illustrated in

Figure 5.2 was constructed and tested. For a given load torque applied to the machine, as the load resistance decreases, the voltage drop across the load decreases.
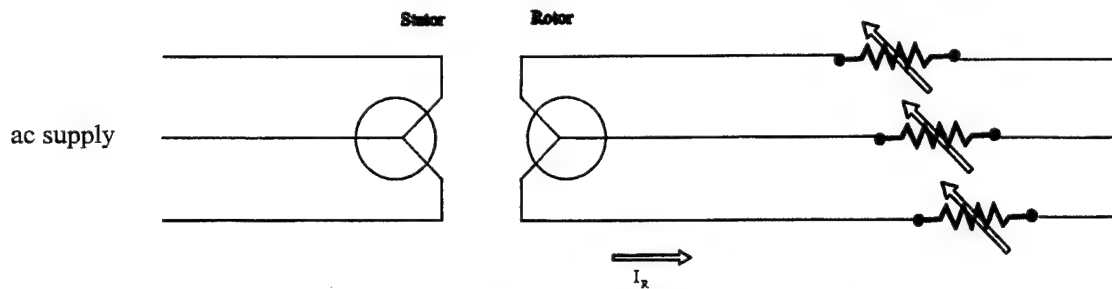

Figure 5.1 Variable Rotor Resistance Scheme

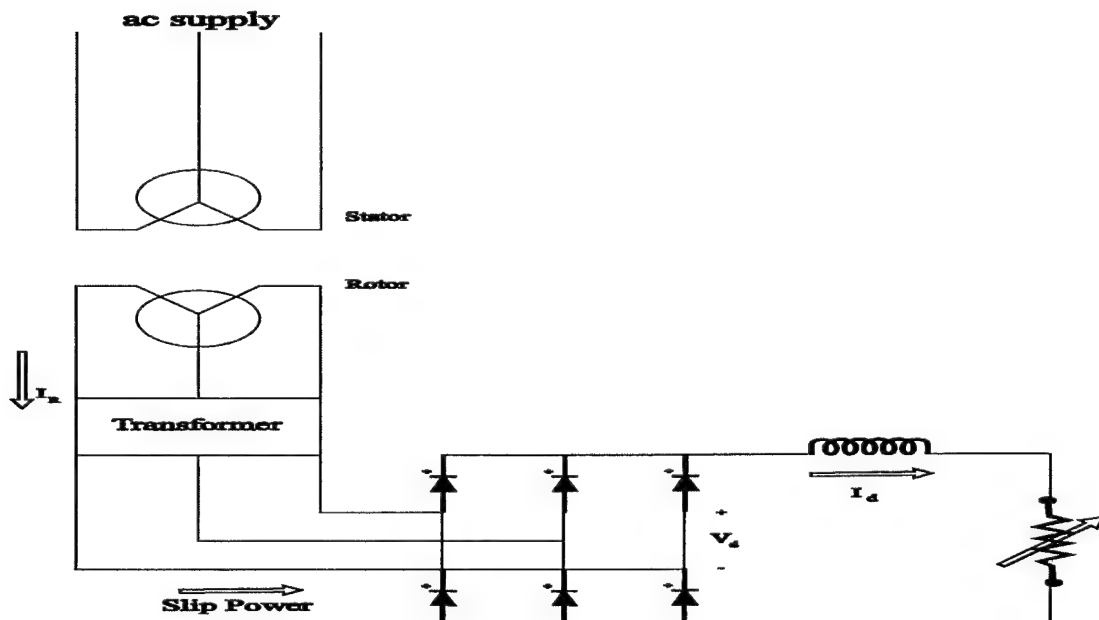Figure 5.2 Diode Bridge with Variable Load Resistance

Since the voltage across the diode bridge and resistor seek to be the same with the inductor current constant, the voltage across the diode bridge also decreases. Thus, the injection counter emf decreases and the motor speed increases. After testing this circuit under various load conditions, it was shown that the rotor could deliver a dc voltage as

great as 50 volts and a dc current in excess of 2 amps. This proved useful in determining

the type and rating of the remaining equipment needed in the SERS.

D. INTEGRATED SYSTEM

The location of the transformer in the SERS proved to be very important. In this

section, the process used to determine the optimal location of the transformer in the SERS

is explained.

1. Transformer on the Rotor-Side

The first location examined for the transformer was on the rotor-side with a ratio

of 1:2. The 1:2 ratio steps up the voltages from the rotor and conversely steps down the

currents out of the rotor. This configuration is illustrated in Figure 5.3.
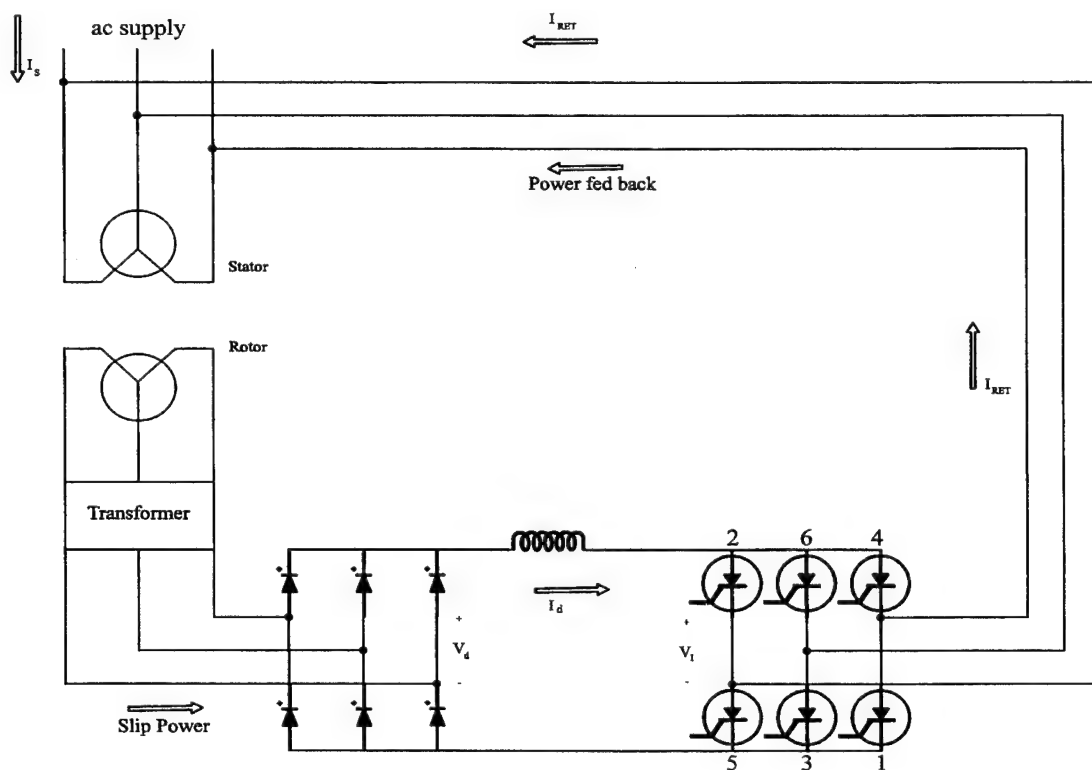

Figure 5.3 Slip Energy Recovery System

Testing for this and subsequent configurations consisted of varying α (as read off of the thyristor firing control unit) from 179.3° to it lowest possible value for various load conditions while being careful not to exceed the current limitations of the equipment. After results were tabulated, torque versus speed graphs were obtained and compared. Figure 5.4 shows the torque versus speed curves while varying α from 179.3° to 146.3°. The different alphas with their associated symbols shown in Figure 5.4 from left to right on the graph are: 179.3° (x), 170.9° (*), 164.5° (+), 159.6° (-), 154.6° (x), 147.7° (o), 146.3° (--). It is noted that this configuration offers a wide speed range (900 rpm) for a given torque and a wide torque range (up to 8 lbf-in) for a given alpha.
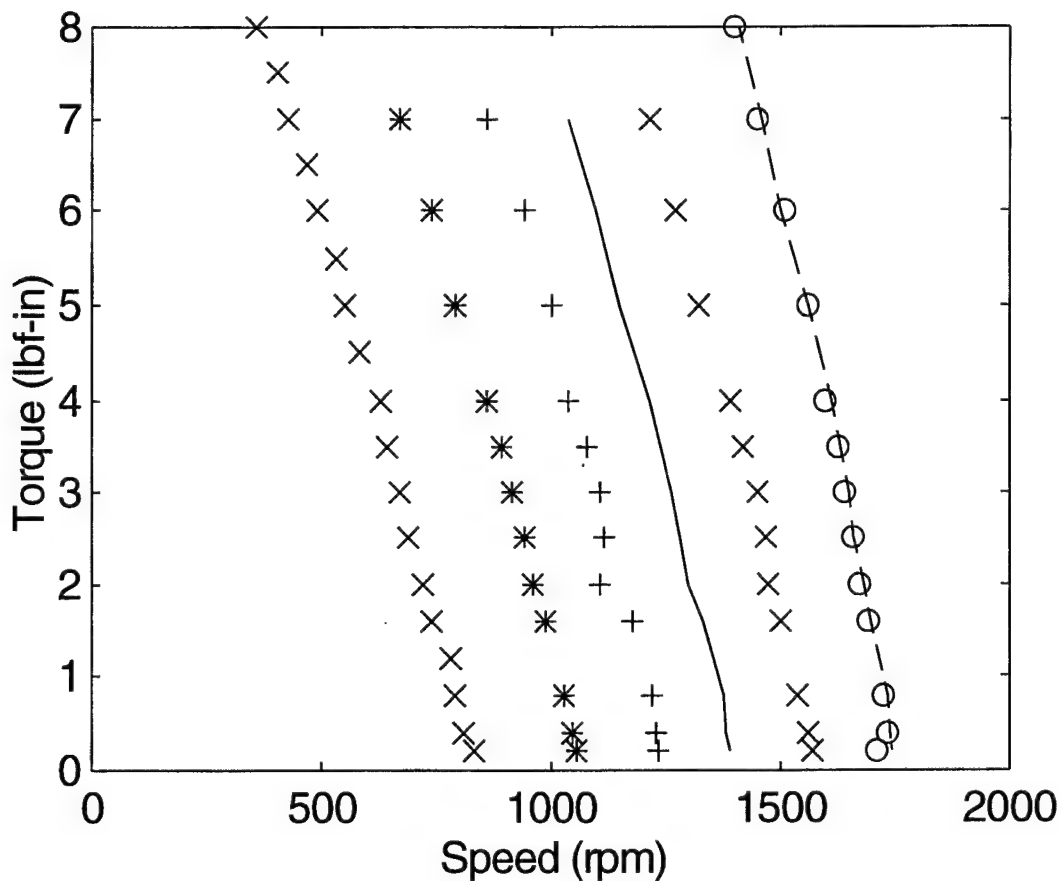

Figure 5.4 Transformer (1:2) on the Rotor-Side for Various α Values

Notice, also, that as α increases for a given torque, the speed of the rotor increases. This can be explained in the following way. As the firing angle, α, of the inverter is increased, the dc voltage across the thyristor inverter decreases which causes the voltage across the diode bridge to decrease. Thus, the injection counter emf decreases and the motor speed increases. When the firing angle is increased, the opposite effect occurs and the motor speed decreases. The limiting element in this circuit is the rotor current limitation of 2 amps which was reached when the load torque was increased to 7 or 8 lbf-in.

This circuit was also tested with the transformer ratio increased to 1:3.5. It was theorized that by increasing the transformer turns ratio, the injection counter emf (onto the rotor) for a given alpha and load would be smaller than that of the previous case. Thus, higher speeds would occur. Figure 5.5 shows a comparison of the 1:2 (x) and 1:3.5 (*) circuits for alpha angles from left to right: 179.3°, 159.6° and 147.7°. Notice that in every case the 1:3.5 curves yield higher speeds for a given load and alpha. Also, notice that as α approaches 146.3°, the speed gap between the two cases is smaller.

2. Transformer on the Inverter-Side

The second location examined for the transformer was on the inverter-side with a ratio of 1:2. Figure 2.1 illustrates the configuration. Figure 5.6 shows a comparison between rotor and inverter-side locations for a transformer with a turns ratio of 1:2 for various alphas and torques. For a given alpha, as the load changes, the corresponding speed is lower for the configuration on the inverter-side as opposed to the rotor-side. That is, for a given alpha and load, the voltage across the diode bridge for the case with

the transformer on the inverter-side must be less than the voltage across the diode bridge with the transformer on the rotor-side. Thus, it follows that the speed will be less for the inverter-side case than for the rotor-side case.
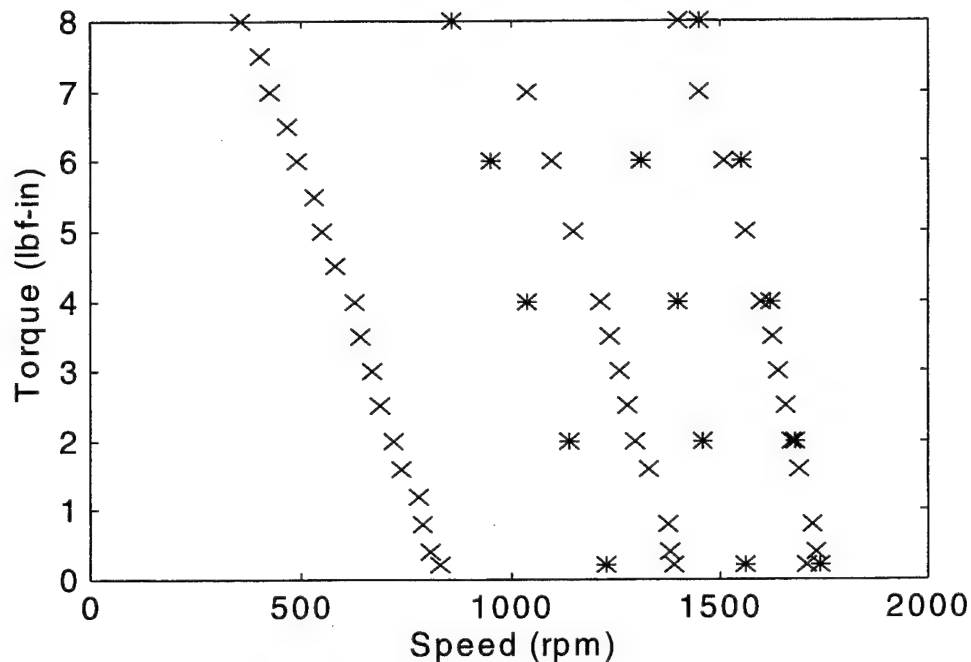
Figure 5.5 Transformer Rotor-Side (1:2) (x) and (1:3.5) (*) for (l-r) $\alpha = 179.3°$, 159.6° and 147.7°.

3. No Transformer

Lastly, the case with no transformer in the circuit was examined. A comparison between no transformer (*) and rotor-side transformer (1:2) (x) was investigated, and the results are shown in Figure 5.7. In Figure 5.7, the alpha angles considered are from left to right: 170.9°, 164.5°, 159.6°, 154.0° and 147.7°. If the motor application requires a large range of speed control, then the no-transformer configuration appears to be the most appropriate one. The no-transformer configuration offers the widest operating range.
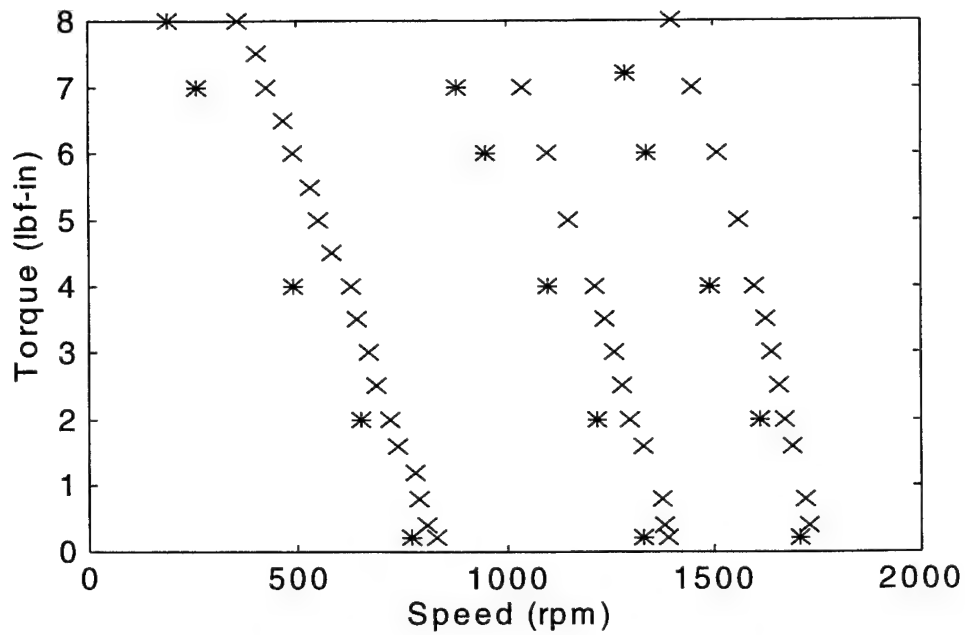
Figure 5.6 Transformer (1:2) on Rotor-Side (x) versus Inverter-Side (*) for (l-r) α = 179.3°, 159.6° and 147.7°.
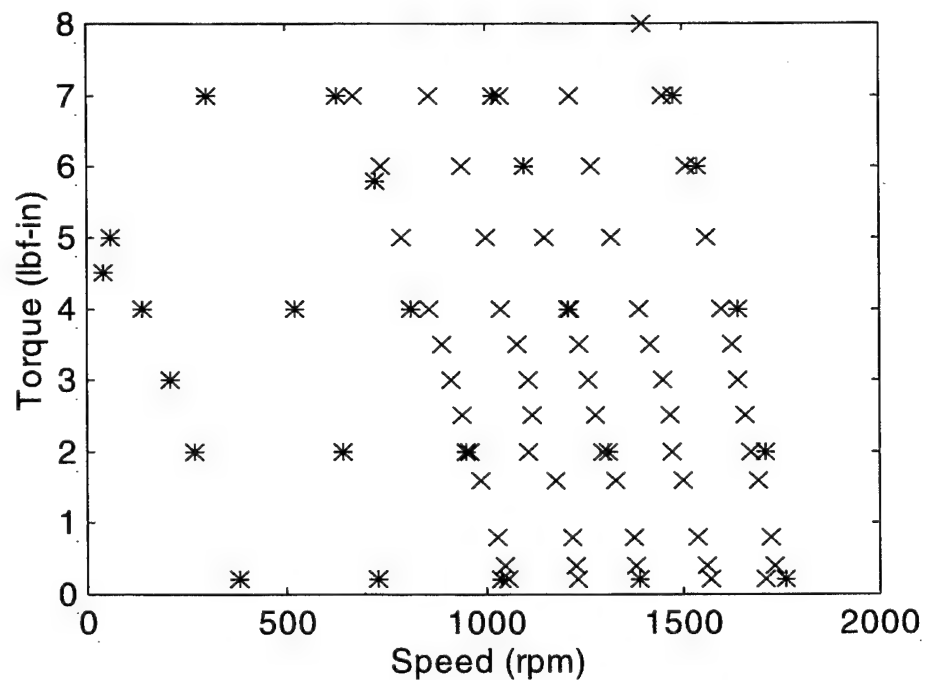
Figure 5.7 Transformer Rotor-Side (1:2) (x) and No-Transformer (*) for (l-r) α = 170.9°, 164.5°, 159.6°, 154.0°, and 147.7°.

41

E. CONCLUSION

In this chapter, preliminary schemes were tested prior to the full implementation of the SERS. A baseline configuration was established. By changing the location and turns ratio of the transformer, comparisons were made between the baseline and other configurations utilizing torque versus speed curves. Because of its wide operating range, the transformer (1:2) on the rotor-side was selected for further testing and control synthesis.

VI. WAVEFORM, POWER FLOW AND EFFICIENCY STUDIES

A. INTRODUCTION

In this chapter, a particular location for the transformer is considered and a set of studies are presented illustrating the operation of the SERS. For a variety of alpha angles and loads, waveforms are analyzed, efficiencies are calculated and discrepancies with the Chapter III analysis are discussed. Finally, conclusions are drawn about power factor and efficiency from the gathered data.

Several alternative configurations of the SERS were investigated and reported on in Chapter V. In reviewing the data collected, it was decided to investigate in detail the configuration that included the transformer on the rotor-side with a 1:2 turns ratio. The transformer effectively provides a boost in rotor voltage which results in a larger diode bridge voltage for a given rotor speed. As a consequence, a larger range of speed control was obtained for the admissible range of thyristor firing control unit angles.

B. WAVEFORMS

In this section, waveforms for the configuration illustrated in Figure 5.3 are presented and discussed. The transformer has a turns ratio of 1:2. The system is investigated during steady-state operation at a variety of firing angles and load torque conditions. Signal waveforms at key locations in the SERS are plotted and contrasted for the different operating conditions. First, a no-load condition is investigated with alpha set at 179.3° and 159.6°. Subsequently, a 4 lbf-in load is considered for the same alpha angles.

43

The following signal waveforms from Figure 5.3 were monitored: rotor voltage (V_R-line-to-line) and current (I_R), transformer voltage (V_T) and current (I_T) on the diode bridge side and, voltage across the diode bridge (V_d), dc link current (I_d), voltage across the inverter (V_I), source phase voltage (V_S) and current (I_S) and feedback current returned to the system (I_{RET}).

1. No-Load Condition

The system was configured as shown in Figure 5.3 with the transformer having a turns ratio of 1:2 and no load applied. With α=179.3°, the system was slowly energized by gradually raising the power supply voltage. This study will be referred to as case 1. The rotor speed increased and steadied out at 820 rpm.

Waveforms for the above conditions are shown in Figures 6.1 through 6.7. Figure 6.1 shows the rotor voltage and current waveforms. Note that the frequency of these waveforms is 33 Hz which corresponds to slip frequency. Note also that the fundamental components of these waveforms are not in phase repudiating the assumption that rotor leakage inductance is negligible. Sinusoidal waveshapes are expected for the voltages because of the nature of the induction machine. The rotor currents are the classical 120° waveshapes anticipated from a six-pulse converter. The superimposed ripple results from the fact that the dc link current is not constant. Note that the peak values are approximately 70 volts for the rotor voltage and 0.3 amps for the rotor current.

Upon leaving the rotor, the signals go through a step-up transformer which boosts the voltage value by a factor of two and reduces the current by the same factor. Figure 6.2 illustrates the transformer action. The line-to-line voltage leaving the

44
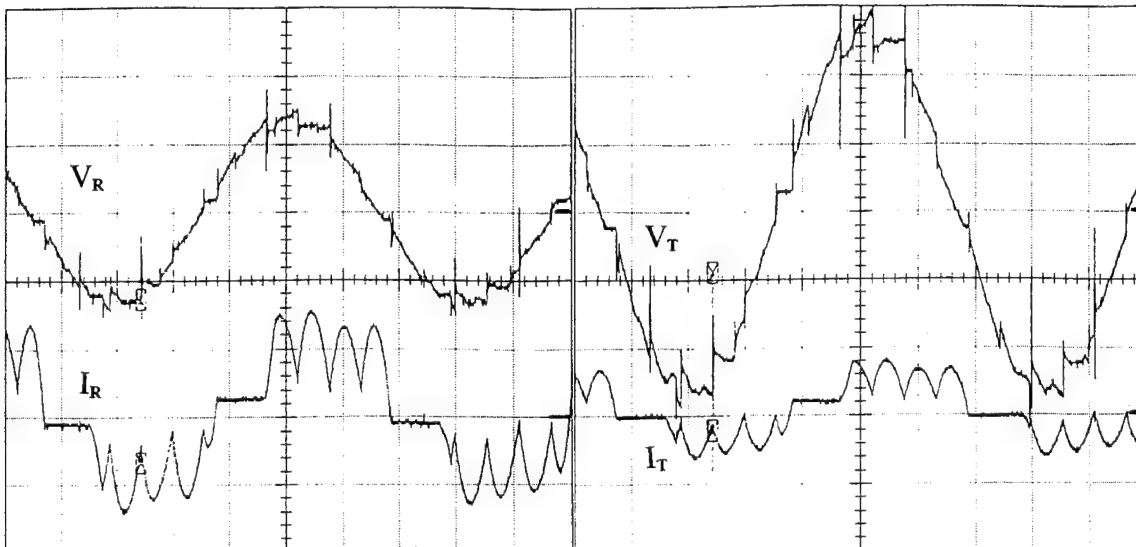
Figure 6.1 Rotor Voltage, V_R (50V/div)
and Rotor Current, I_R (0.2A/div) vs.
Time (5ms/div); α=179.3°, T_L=0 lbf-in

Figure 6.2 Transformer Voltage, V_T
(50V/div) and Transformer Current, I_T
(0.2A/div) vs. Time (5ms/div); α=179.3°,
T_L=0 lbf-in
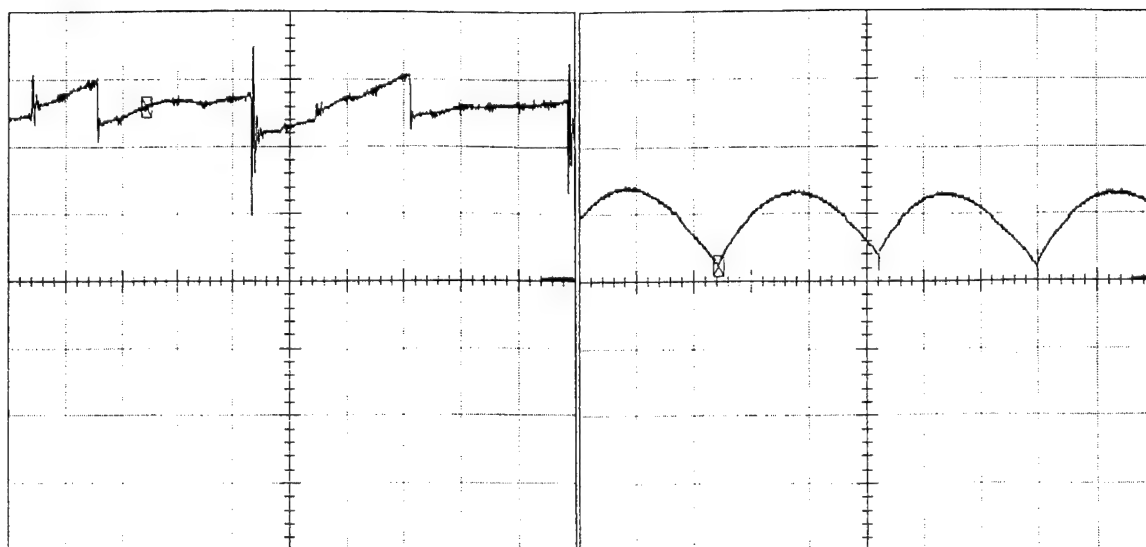
Figure 6.3 Diode Bridge Voltage, V_d
(50V/div) vs. Time (1ms/div); α=179.3°,
T_L=0 lbf-in

Figure 6.4 DC Link Current, I_d
(0.1A/div) vs. Time (1ms/div); α=179.3°,
T_L=0 lbf-in

45

Figure 6.5 Inverter Voltage, V_I
(100V/div) vs. Time (1ms/div);
α=179.3°, T_L=0 lbf-in

Figure 6.6 Source Phase Voltage, V_s
(100V/div) vs. Time (5ms/div);
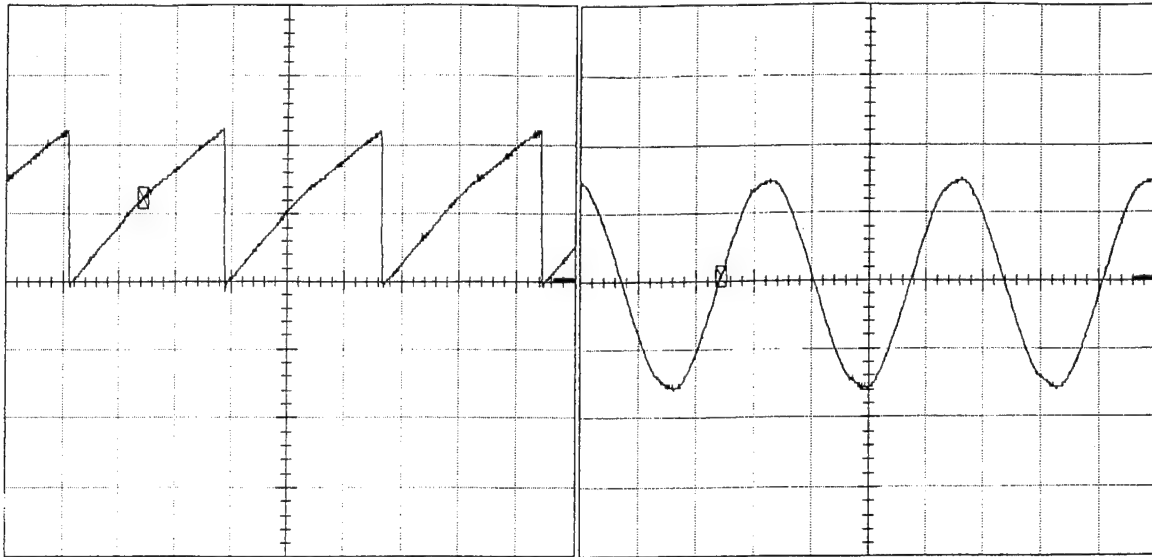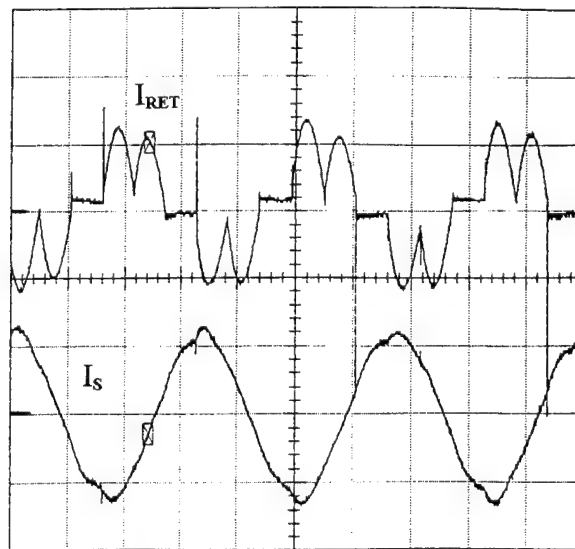α=179.3°, T_L=0 lbf-in

Figure 6.7 Return Current, I_{RET}
(0.1A/div) and Source Phase Current, I_s
(1A/div) vs. Time (5ms/div); α=179.3°,
T_L=0 lbf-in

46

transformer is approximately 150 volts peak and the current is 0.16 amps peak. The diode bridge rectifies the sinusoidal voltage waveform provided by the transformer (shown in Figure 6.3). The average voltage across the diode bridge (V_d) is about 130 volts.

The dc link current, I_d, is illustrated in Figure 6.4. Ideally, this waveform should be a flat dc value, but in Figure 6.4, some ripple is clearly present. The dc link current has a peak value of 0.14 amps. The peak-to-peak ripple is 0.1 amps and occurs at a frequency of 360 Hz, six times the line frequency.

With the system operating at α=179.3°, the average voltage across the inverter is at its maximum value. The V_I waveform, shown in Figure 6.5, ranges from zero volts to 240 volts with a mean value of approximately 130 volts. This is expected since V_I and V_d must balance as discussed in Chapter III. The frequency of the inverter ripple voltage is 360 Hz, consistent with a six-pulse converter connected to a 60 Hz source. The stator phase voltage and current along with current returned to the system are illustrated in Figures 6.6 and 6.7. The source phase voltage (l-n), shown in Figure 6.6, is sinusoidal without much distortion and has a peak amplitude of 150 volts. The source phase currents are slightly distorted from the pseudo-rectangular current waveforms delivered by the six-pulse converter. The source current amplitude is approximately 1.2 amps. The return current waveshape, I_{RET}, is depicted in Figure 6.7 and appears as an unfolded version of I_d. It is unfolded by the inverter, so considering the two currents, the return current waveshape is anticipated. Its peak value is 0.13 amps.

47

Still considering no-load operation, alpha was next changed to 159.6°. This study will be referred to as case 2. Waveforms for this case are given in Figures 6.8 through 6.14. At this alpha, the steady-state motor speed has increased to 1380 rpm. Since the rotor is running closer to synchronous speed, the induced rotor voltages must have a lower amplitude than in the previous case. As shown in Figure 6.8, the rotor voltage is noticeably lower and the rotor current amplitude is about the same as in the previous case. The V_R peak is about 35 volts with the frequency being about 13 Hz (slip frequency). Figure 6.9 illustrates the signal waveshapes between the transformer and diode bridge.

Figure 6.10 shows the voltage across the diode bridge which has a peak value of 70 volts while the average value is on the order of 50 volts. With alpha decreasing from the previous point, the average voltage across the inverter must decrease and balance out the lower diode bridge average voltage. The dc link current may be viewed in Figure 6.11. The link current has a slightly smaller peak value than in the previous case with the frequency of the ripple current maintained at 360 Hz.

The inverter voltage is shown in Figure 6.12. By decreasing alpha, the average voltage across the inverter is made smaller. The voltage values range from -80 volts to 180 volts. With the waveshape being nearly triangular, the average value is estimated at 50 volts. As anticipated, this value coincides closely with the average value out of the diode bridge.

Figures 6.13 and 6.14 illustrate insignificant changes in the source voltage, source current and return current at the new value of alpha. It is instructive to note that the

48

Figure 6.8 Rotor Voltage, V_R (20V/div) and Rotor Current, I_R (0.2A/div) vs. Time (10ms/div); $\alpha=159.6°$, $T_L=0$ lbf-in

Figure 6.9 Transformer Voltage, V_T (50V/div) and Transformer Current, I_T (0.2A/div) vs. Time (10ms/div); $\alpha=159.6°$, $T_L=0$ lbf-in

Figure 6.10 Diode Bridge Voltage, V_d (50V/div) vs. Time (1ms/div); $\alpha=159.6°$, $T_L=0$ lbf-in
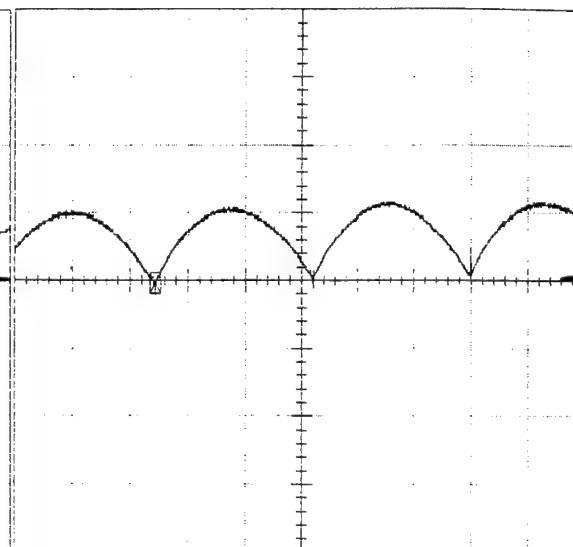
Figure 6.11 DC Link Current, I_d (0.1A/div) vs. Time (1ms/div); $\alpha=159.6°$, $T_L=0$ lbf-in

49

Figure 6.12 Inverter Voltage, V_I
(100V/div) vs. Time (1ms/div);
α=159.6°, T_L=0 lbf-in

Figure 6.13 Source Phase Voltage, V_s
(100V/div) vs. Time (5ms/div);
α=159.6°, T_L=0 lbf-in

Figure 6.14 Return Current, I_{RET}
(0.1A/div) and Source Phase Current, I_s
(1A/div) vs. Time (5ms/div); α=159.6°,
T_L=0 lbf-in

50

return current always has two humps for a given half cycle. When the system is loaded, these waveforms will, however, change appreciably.

2. Loaded Condition

Having viewed waveforms for two different alpha angles for a no-load condition, the next step is to view the same waveforms with the same alpha angles but with a load attached. When a load is attached to an induction machine, larger rotor currents flow to produce the torque necessary to drive the load. As discussed in Chapter III, the rotor current is proportional to the link current. Thus, as rotor current increases, the dc link current must increase. If the link current is higher, then, the return current must be higher also.

With the system operating in steady state and $\alpha=179.3°$, a 4 lbf-in load is applied to the rotor through a dynamometer and belt arrangement. This study will be referred to as case 3. The speed of the machine slows to a steady value of 620 rpm. The waveforms for this case are shown in Figures 6.15 through 6.21.

When compared with the $\alpha=179.3°$ and the no-load case, case 1, the waveforms captured show results as expected. The difference between the current values is very noticeable. For example, Figure 6.15 shows I_R at a peak value of 1.1 amps as compared to the case 1 peak rotor current value of 0.3 amps. This increase in current is reflected throughout the system and is seen by increases in link and returned currents in Figures 6.18 and 6.21, respectively. In particular, they increase to peak values of 0.4 and 0.6 amps. An increase in the distortion of the source phase current is clearly evident in
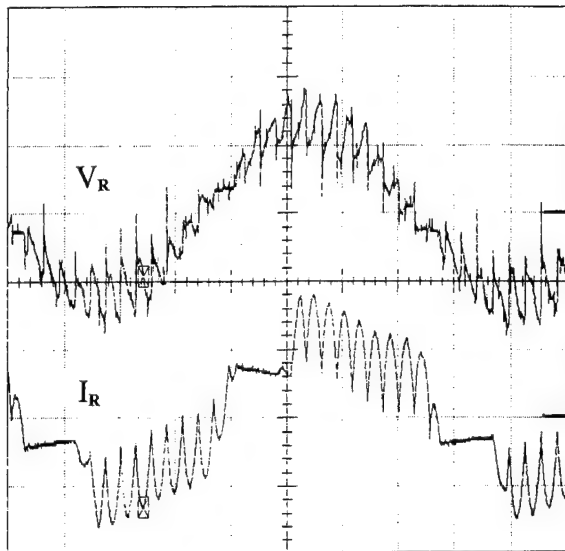
51

Figure 6.15 Rotor Voltage, V_R (50V/div)
and Rotor Current, I_R (1A/div) vs. Time
(5ms/div); $\alpha=179.3°$, $T_L=4$ lbf-in

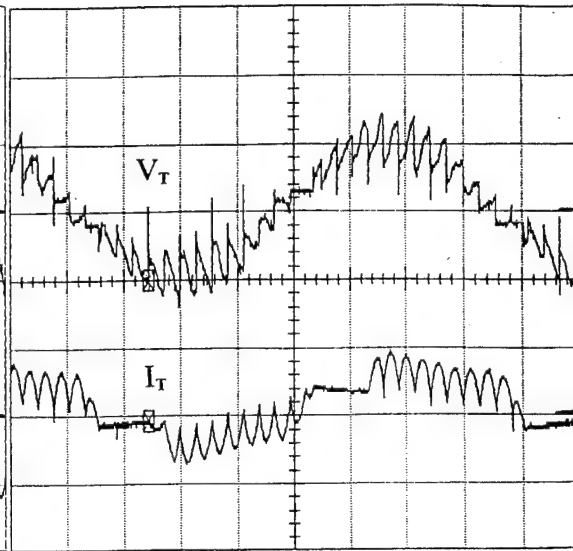

Figure 6.16 Transformer Voltage, V_T
(50V/div) and Transformer Current, I_T
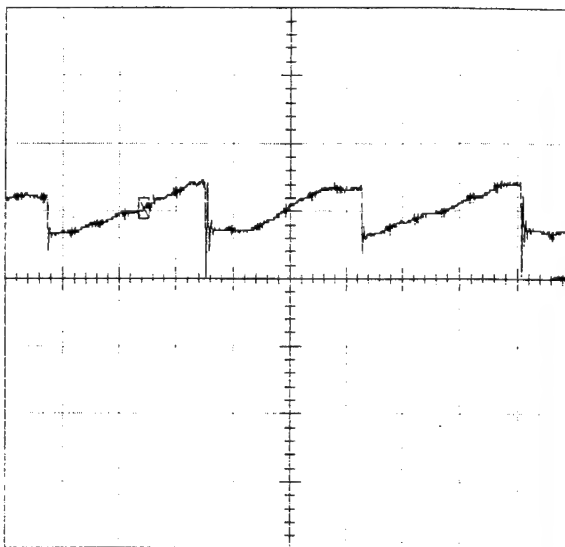(1A/div) vs. Time (5ms/div); $\alpha=179.3°$,
$T_L=4$ lbf-in

Figure 6.17 Diode Bridge Voltage, V_d
(50V/div) vs. Time (1ms/div); $\alpha=179.3°$,
$T_L=4$ lbf-in

Figure 6.18 DC Link Current, I_d
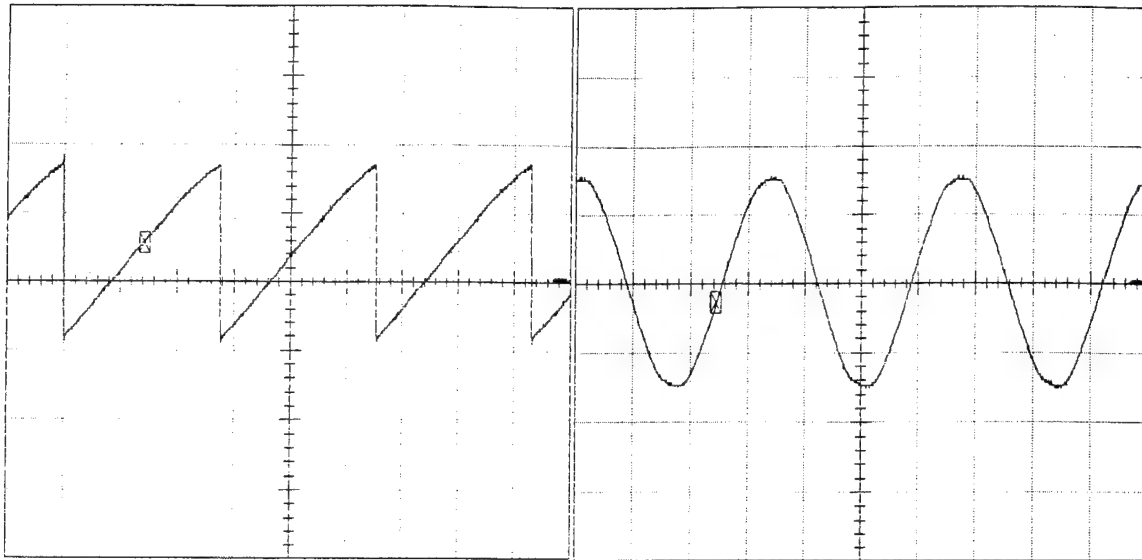(0.2A/div) vs. Time (1ms/div); $\alpha=179.3°$,
$T_L=4$ lbf-in

52
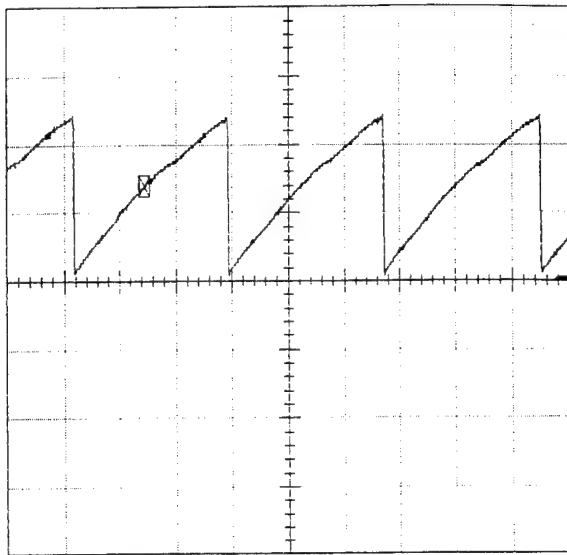
Figure 6.19 Inverter Voltage, V_I
(100V/div) vs. Time (1ms/div);
α=179.3°, T_L=4 lbf-in

Figure 6.20 Source Phase Voltage, V_s
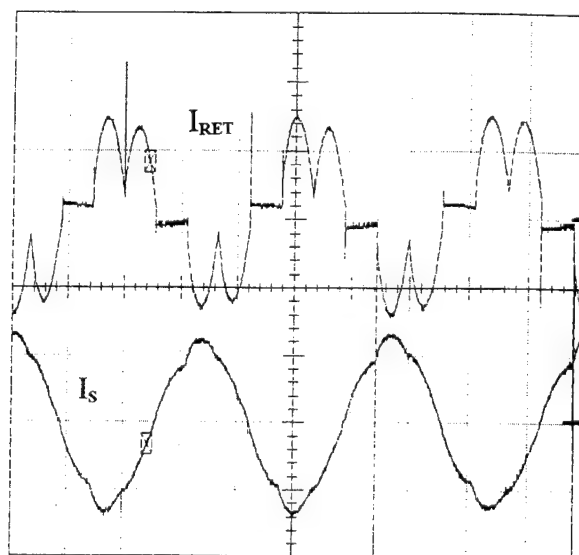(100V/div) vs. Time (5ms/div);
α=179.3°, T_L=4 lbf-in

Figure 6.21 Return Current, I_{RET}
(1A/div) and Source Phase Current, I_s
(1A/div) vs. Time (5ms/div); α=179.3°,
T_L=4 lbf-in

Figure 6.21. This is due to harmonics being introduced into the system by the larger return current.

When compared with case 1, voltage values in case 3 are similar because the inverter via the firing angle will uniquely dictate these levels (except for the stator source voltage). Also, a comparison at different load conditions shows that the source commutating inductance does not appear to play an observable role in the system or does not impact the average value of the inverter voltage.

The fourth and final case has α=159.6° and a 4 lbf-in load attached to the rotor. The machine speed slows from the no-load speed of 1380 rpm and steadies out at 1220 rpm. Waveforms for this case are illustrated in Figures 6.22 through 6.28.

As in the previous case, the rotor current is noticeably higher than that observed in case 2 with the same alpha angle and no load. This increase, again, is reflected throughout the system. The peak values of rotor, link and return currents are 1.0, 0.45, and 0.6 amps, respectively. These are shown in Figures 6.22, 6.25 and 6.26. In Figure 6.28, the source current appears to be more distorted than in the previous case. This makes sense since more reactive power is being absorbed by the inverter when alpha is at a lower value. This holds because the power factor angle at α=179.3° is roughly -60.7° while the power factor angle at α=159.6° is roughly -80.4°. Since the reactive power varies as the sine of the power factor angle, reactive power absorbed by the inverter increases with decreases in α.

Comparison of the voltage levels found in case 4 and case 2 indicate that they are very similar. Figures 6.8 and 6.22 show the rotor voltage and both illustrate peak values
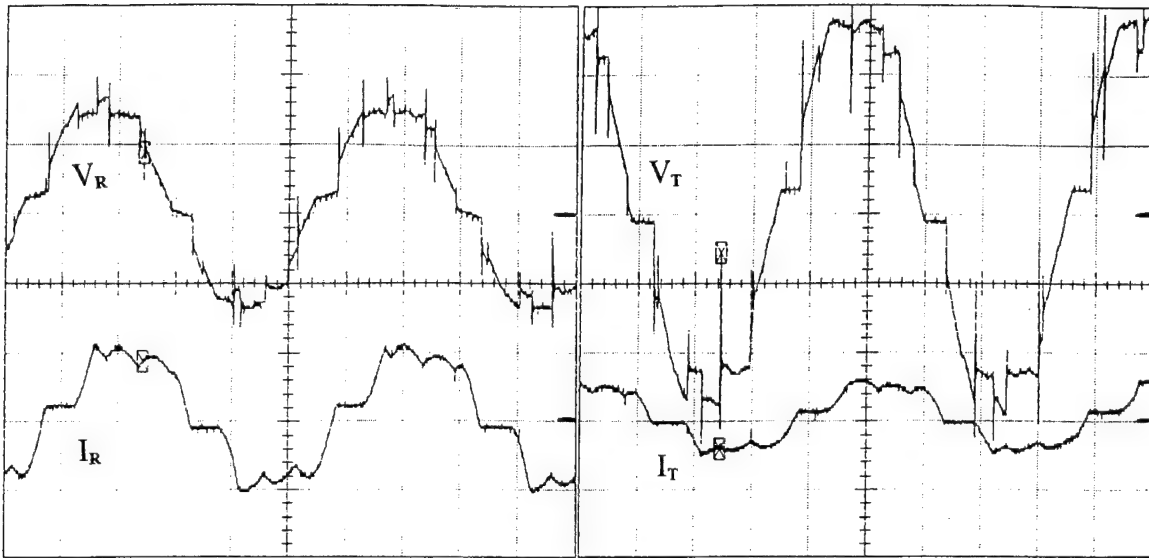
54
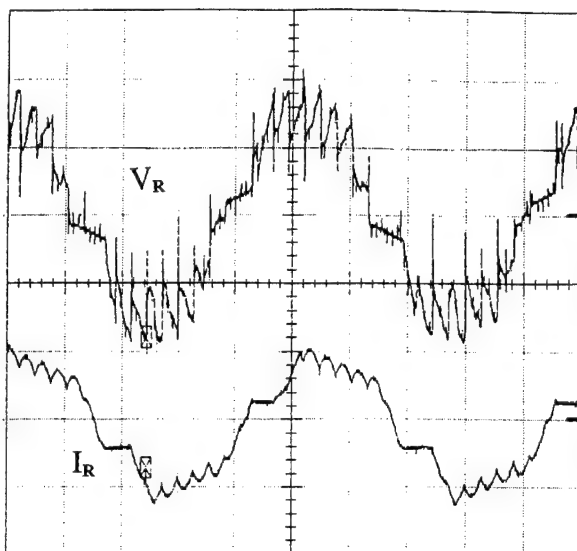
Figure 6.22 Rotor Voltage, V_R (20V/div) and Rotor Current, I_R (1A/div) vs. Time (10ms/div); $\alpha=159.6°$, $T_L=4$ lbf-in
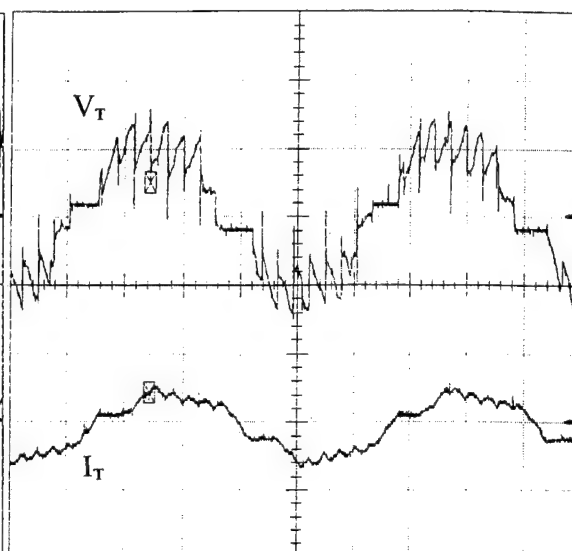
Figure 6.23 Transformer Voltage, V_T (50V/div) and Transformer Current, I_T (1A/div) vs. Time (10ms/div); $\alpha=159.6°$, $T_L=4$ lbf-in
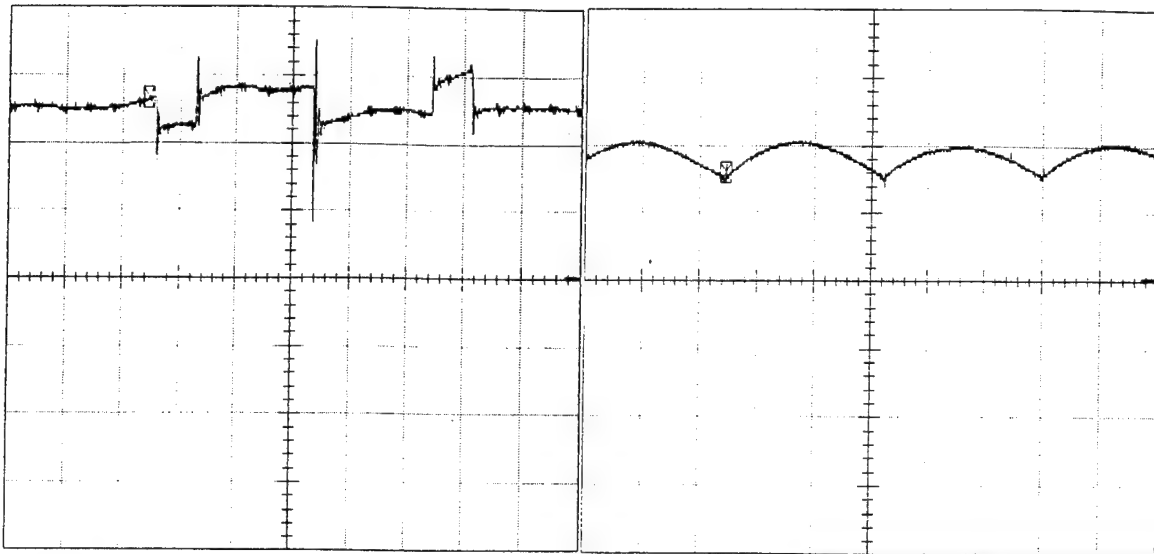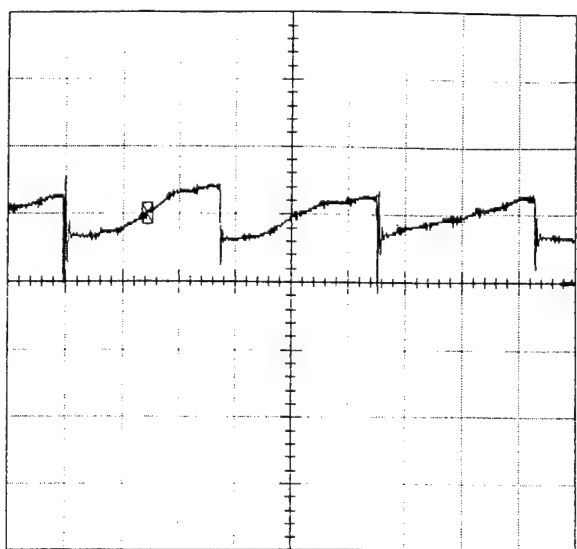

Figure 6.24 Diode Bridge Voltage, V_d (50V/div) vs. Time (1ms/div); $\alpha=159.6°$, $T_L=4$ lbf-in
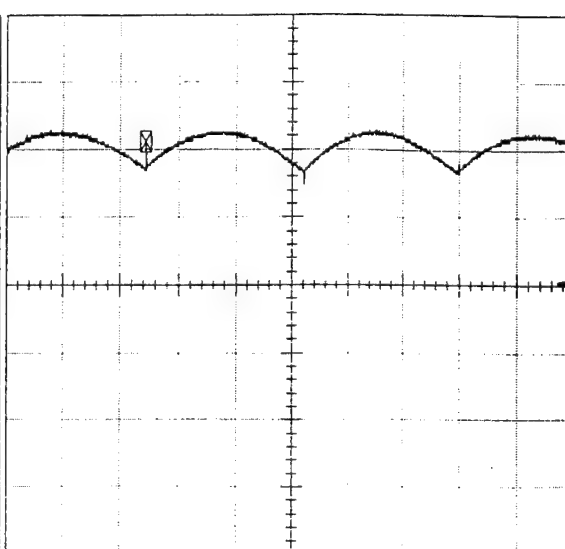
Figure 6.25 DC Link Current, I_d (0.2A/div) vs. Time (1ms/div); $\alpha=159.6°$, $T_L=4$ lbf-in

55
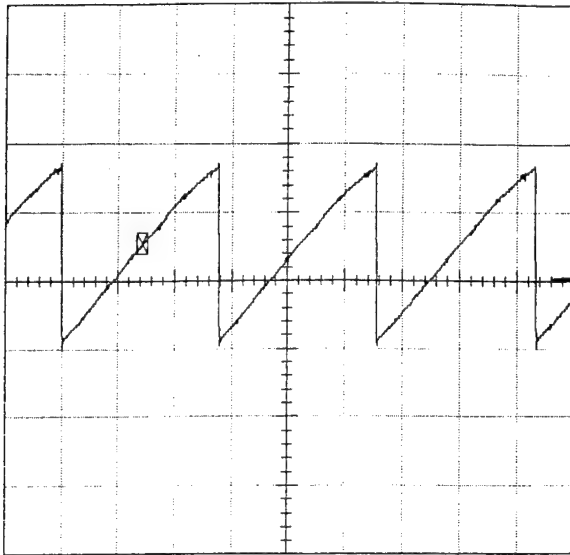
Figure 6.26 Inverter Voltage, V_I
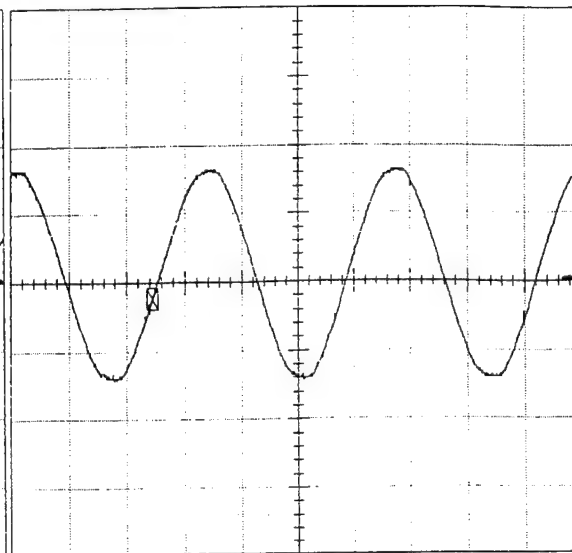(100V/div) vs. Time (1ms/div);
α=159.6°, T_L=4 lbf-in
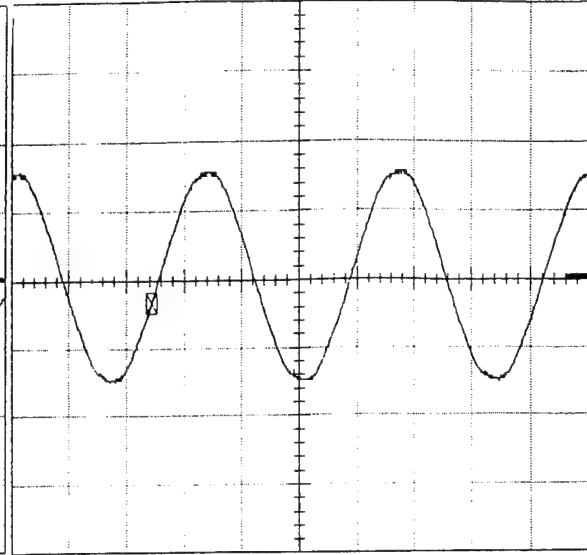
Figure 6.27 Source Phase Voltage, V_s
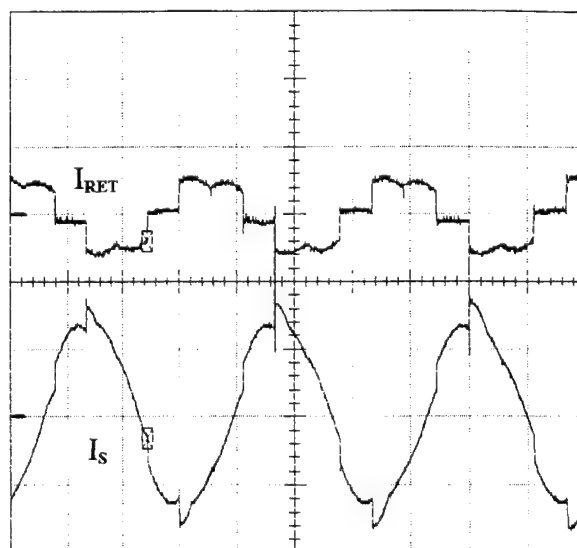(100V/div) vs. Time (5ms/div);
α=159.6°, T_L=4 lbf-in
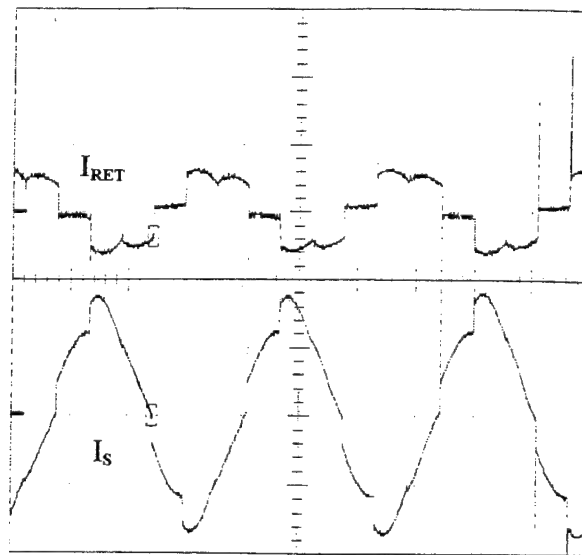
Figure 6.28 Return Current, I_{RET}
(1A/div) and Source Phase Current, I_s
(1A/div) vs. Time (5ms/div); α=159.6°,
T_L=4 lbf-in

56

of 35 to 40 volts. Figures 6.10 and 6.24 show the diode bridge peak voltage at 70 volts.

Figures 6.12 and 6.26 show the inverter peak voltage at roughly the same value. Lastly,

Figures 6.13 and 6.27 display the source phase voltages which appear identical.

While current levels between case 3 and case 4 are not very different, the rotor-

side and link-side voltage levels are noticeably different just as in the comparison of cases

1 and 2. As before, the differences can be attributed to the difference in the alpha firing

angle.

C. EFFICIENCY

1. Introduction

As stated in Chapter III, the efficiency observed for the SERS is much lower than

that anticipated though additional studies at higher load torques may indicate substantial

improvement. The low power factor observed in the SERS is expected. In this section,

the power factor for the configuration shown in Figure 5.3 for the conditions discussed in

the previous section and two additional conditions are investigated. Data are presented

and calculations are documented to determine the power flow and the power factor for

the system, inverter and motor. Conclusions are drawn from the calculations and

premises introduced in Chapter III.

2. Calculations

The three different power factors considered are Pf_{sys}, Pf_{inv} and Pf_{motor}. Power

factor, Pf, can be expressed as

$$Pf = \frac{\text{Real Power } (P)}{\text{Apparent Power } (S)} \qquad (6.1)$$

57

The two watt meter method was used to arrive at the total 3-phase real power delivered by the source, P_{sys}, and returned by the inverter, P_{inv}. Knowing two of the three powers at the junction, the third, real power into the motor, P_{motor}, can be deduced from

$$P_{motor} = P_{sys} + P_{inv} \qquad (6.2)$$

This illustrates where the improvement in SERS efficiency is obtained. Clearly with real power being returned from the inverter, the system does not need to deliver as much for a given motor input power demand. With α_o ranging from $90°$ to $180°$, this implies that the admissible power factor angles range from $-90°$ to $0°$. Thus, since the real power delivered by the inverter varies as the cosine of the power factor angle, P_{inv} should be maximum when α_o (or α) is maximum.

Knowing the real power, the reactive power is obtained once the apparent power is calculated. The apparent power is found by measuring the rms phase current and rms line-to-line voltage and can be expressed as

$$S = \sqrt{3} \, I_p \, V_{l-l} \qquad (6.3)$$

where I_p is the rms phase current and V_{l-l} is the rms line-to-line voltage. The reactive powers, Q, delivered to the system and absorbed by the inverter are then calculated by

$$Q = \sqrt{\left(S^2 - P^2\right)} \qquad (6.4)$$

The reactive power absorbed by the motor is then found from

$$Q_{sys} = Q_{motor} + Q_{inv} \qquad (6.5)$$

Equation 6.5 indicates why the power factor of a SERS is normally low. For the range of admissible alphas, Q_{inv} is always positive, and thus this imposes a larger reactive

58

power requirement on the source. Having values for P and S for each element, the component power factors can be determined, conclusions can be drawn on operating efficiency, and characteristics can be assessed. Knowing the load torque applied, motor speed, and the system input power, system efficiency is calculated as

$$\text{Efficiency}\% = \frac{\text{mechanical power out}}{\text{electrical power in}\,(\text{P}_{\text{sys}})} * 100 \qquad (6.6)$$

where

$$\text{P}_{\text{mech out}}(W) = T_L(lbf\text{-}in)\left(\frac{1\,ft}{12\,in}\right)\left(\frac{1\,N-m}{0.738\,lb-ft}\right)(\omega_{\text{rm}}(rpm))\left(\frac{2\pi}{60}\right) \qquad (6.7)$$

3. Data

In the previous section, four cases with differing operating conditions were considered. For this section, an additional load condition, 2.0 lbf-in, is included for each alpha angle. The data for the a-phase and c-phase were collected and are listed in Tables 6.1 through 6.6.

4. Results

The power flow and efficiency results are tabulated using Equations 6.1 through 6.7 and are documented in Tables 6.7 through 6.9. Note that the power calculations were performed using the data from both line measurements, hence, the aϕ and cϕ results.

5. Conclusions

From Tables 6.7 through 6.9, some conclusions are drawn. First, as mentioned in Chapter III, as the delay angle alpha decreases, the inverter real power returned decreases and the reactive power absorbed increases. Thus, Pf_{inv} decreases. Second, real supplied power increases more than reactive power supplied to the system when the machine

59

operates at a higher speed and with a larger load torque. Third, as the machine is loaded, the increase in real power drawn by the machine is greater than the increase in reactive power drawn by the machine. For these reasons, the SERS operates most efficiently at higher speeds and larger load torques.

Supply	A ϕ	C ϕ
Iϕ (A$_{rms}$)	0.750	0.744
V$_{l-l}$ (V$_{rms}$)	184.1	184.3
Pϕ (W)	- 46.3	89.5
Return	A ϕ	C ϕ
Iϕ (A$_{rms}$)	0.080	0.079
V$_{l-l}$ (V$_{rms}$)	184.4	184.7
Pϕ (W)	10.6	- 0.6

Table 6.1 Data for Load = 0 lbf-in; α = 179.3°; rotor speed = 820 rpm

Supply	A ϕ	C ϕ
Iϕ (A$_{rms}$)	0.771	0.765
V$_{l-l}$ (V$_{rms}$)	184.9	185.0
Pϕ (W)	- 43.2	92.5
Return	A ϕ	C ϕ
Iϕ (A$_{rms}$)	0.094	0.093
V$_{l-l}$ (V$_{rms}$)	184.5	184.7
Pϕ (W)	9.4	- 5.7

Table 6.2 Data for Load = 0 lbf-in; α = 159.6°; rotor speed = 1380 rpm

Supply	A φ	C φ
Iφ (A$_{rms}$)	0.870	0.866
V$_{l-l}$ (V$_{rms}$)	184.9	184.9
Pφ (W)	- 46.2	111.0
Return	A φ	C φ
Iφ (A$_{rms}$)	0.207	0.208
V$_{l-l}$ (V$_{rms}$)	184.7	185.0
Pφ (W)	30.9	- 0.8

Table 6.3 Data for Load = 2.0 lbf-in; α = 179.3°; rotor speed = 730 rpm

Supply	A φ	C φ
Iφ (A$_{rms}$)	0.918	0.912
V$_{l-l}$ (V$_{rms}$)	184.8	184.7
Pφ (W)	- 36.5	124.5
Return	A φ	C φ
Iφ (A$_{rms}$)	0.230	0.228
V$_{l-l}$ (V$_{rms}$)	184.6	184.6
Pφ (W)	25.1	- 13.4

Table 6.4 Data for Load = 2.0 lbf-in; α = 159.6°; rotor speed = 1310 rpm

Supply	A ϕ	C ϕ
Iϕ (A$_{rms}$)	1.028	1.020
V$_{l-l}$ (V$_{rms}$)	185.0	185.3
Pϕ (W)	- 46.6	135.7
Return	A ϕ	C ϕ
Iϕ (A$_{rms}$)	0.359	0.358
V$_{l-l}$ (V$_{rms}$)	185.1	185.3
Pϕ (W)	54.6	- 1.1

Table 6.5 Data for Load = 4.0 lbf-in; α = 179.3°; rotor speed = 620 rpm

Supply	A ϕ	C ϕ
Iϕ (A$_{rms}$)	1.091	1.088
V$_{l-l}$ (V$_{rms}$)	185.4	185.5
Pϕ (W)	- 31.2	159.0
Return	A ϕ	C ϕ
Iϕ (A$_{rms}$)	0.372	0.373
V$_{l-l}$ (V$_{rms}$)	185.2	185.4
Pϕ (W)	41.8	- 22.4

Table 6.6 Data for Load = 4.0 lbf-in; α = 159.6°; rotor speed = 1220 rpm

A φ						
Case	1	2	3	4	5	6
	α=179.3°	α=159.6°	α=179.3°	α=159.6°	α=179.3°	α=159.6°
Speed	820 rpm	1380 rpm	730 rpm	1310 rpm	620 rpm	1220 rpm
(lbf-in)	$T_L = 0$	$T_L = 0$	$T_L = 2.0$	$T_L = 2.0$	$T_L = 4.0$	$T_L = 4.0$
Inv						
P_{inv}	10	3.7	30.1	11.7	53.5	19.4
Q_{inv}	23.5	29.8	58.98	72.6	101.9	117.74
Pf_{inv}	0.391	0.123	0.455	0.159	0.465	0.163
Sys						
P_{sys}	43.2	49.3	64.9	88.0	89.10	127.8
Q_{sys}	235.2	242.0	270.98	280.35	317.12	326.20
Pf_{sys}	0.181	0.199	0.233	0.299	0.271	0.365
Motor						
P_{motor}	53.2	53.0	94.9	99.7	142.6	147.2
Q_{motor}	211.7	213.0	212.0	207.74	215.22	208.46
Pf_{motor}	0.244	0.243	0.409	0.433	0.552	0.577

Table 6.7 Power Calculations A φ

C φ						
Case	1	2	3	4	5	6
	α=179.3°	α=159.6°	α=179.3°	α=159.6°	α=179.3°	α=159.6°
Speed	820 rpm	1380 rpm	730 rpm	1310 rpm	620 rpm	1220 rpm
(lbf-in)	$T_L = 0$	$T_L = 0$	$T_L = 2.0$	$T_L = 2.0$	$T_L = 4.0$	$T_L = 4.0$
Inv						
P_{inv}	10	3.7	30.1	11.7	53.5	19.4
Q_{inv}	23.2	29.5	59.5	72.0	101.6	118.2
Pf_{inv}	0.396	0.124	0.452	0.161	0.466	0.162
Sys						
P_{sys}	43.2	49.3	64.8	88.0	89.1	127.8
Q_{sys}	243.26	240.12	276.25	278.17	315.01	325.37
Pf_{sys}	0.178	0.201	0.222	0.302	0.272	0.366
Motor						
P_{motor}	53.2	53.0	94.9	99.7	142.6	147.2
Q_{motor}	220.06	210.6	216.78	206.22	213.33	207.17
Pf_{motor}	0.235	0.244	0.401	0.435	0.556	0.579

Table 6.8 Power Calculations C φ

System Efficiency				
Case	3	4	5	6
Eff (%)	26.64	35.21	32.91	45.15

Table 6.9 System Efficiency

D. EQUATION VALIDATION

In Chapter II, section C, a steady-state analysis of the SERS was performed. In this section, the dc link equations, Equations 3.22, 3.23 and 3.25, are validated against the corresponding data measurements. In calculating predicted versus actual values, alpha of the thyristor firing control unit, α, is utilized. Equation 2.2 is needed to transform the alpha of the equations used in Chapter III, α_o, into alpha of the firing unit, α.

The system shown in Figure 5.3 was operated at two α_o angle conditions, 109.5° and 99.6°. For each alpha angle, two loads are considered. The resultant data are listed in Table 6.10.

	$\alpha_o = 109.5°$		$\alpha_o = 99.6°$	
Case	1	2	3	4
T_L (lbf-in)	2.0	4.0	2.0	4.0
$V_{s (l-l)}$	183.6	183.9	183.7	183.9
$I\phi$	0.929	1.102	0.928	1.130
V_I	- 86.52	- 86.94	- 46.3	- 46.3
V_d	88.02	89.07	47.11	48.44
I_d	0.31	0.5	0.3	0.5
Rotor Speed (RPM)	1000	910	1310	1220

Table 6.10 Steady-State Analysis Data

64

Using the equations developed in Chapter III, predicted system voltages are derived. These are then compared with actual system values shown in Table 6.10. Conclusions are drawn regarding the slight discrepancy between the two and are discussed in the following paragraphs.

The average diode bridge voltage was analyzed first. Using Equation 3.25, slip for case 1 is calculated as 0.3338. Substituting this slip value into Equation 3.22 and converting the stator line-to-line voltage into a phase voltage, a predicted average dc voltage of 82.7 volts is established. Using the same procedure, the inverter voltage governed by Equation 3.23 is found to be -82.76 volts. The actual measured values for case 1 are shown in Table 6.10. The data for case 1 show that in fact V_I does not equal V_d. This may be explained by ohmic losses in the link inductor. Equation 3.19 can be modified to

$$V_d + V_I - V_{IND} = 0 \qquad\qquad (6.8)$$

Thus, V_{IND} would 1.5 volts. With the case 1 inductor current in Table 5.10 and the V=IR relationship, the inductor resistance is 4.84 Ω. In Chapter IV, the measured inductor resistance was found to be 4.69Ω, and using the inductor current shown in Table 6.10, the voltage drop across the inductor is 1.45 volts.

The process was repeated for case 4. Using equations formulated in Chapter III, predicted values were calculated for slip, V_d, and V_I. For V_d and V_I, the predicted versus actual voltage values were 41.41, 48.44 and -41.41, -46.3, respectively. Using the actual voltage values and substituting them into Equation 6.8 yields an inductor voltage drop of 2.14 volts. Given the case 4 inductor current, inductor resistance is calculated to be 4.28

Ω. Using the measured inductor resistance and current values, in case 4, the voltage drop across the inductor is calculated to be 2.35 volts. In both cases, inductor resistances and voltage drops are of similar values.

E. CONCLUSION

In this chapter, additional waveform, efficiency and power flow studies of the SERS were conducted. Through numerous test sequences, waveforms were analyzed and compared. Data taken during this period provided insight into power flow in the SERS. System efficiency, theorized to be poor, was confirmed to be low although greater efficiency was obtained by loading the system and lowering alpha. Finally, system equations were verified and were found to accurately predict actual in-lab conditions.

VII. ANALOG AND DSPACE CONTROLLERS

A. INTRODUCTION

In this chapter, the closed-loop speed controllers implemented in this research effort are discussed. As introduced in Chapter II, the standard means of adjusting the thyristor-inverter firing angle was the manual adjustment of the dc voltage control knob on the thyristor firing unit control panel. Once the firing control angle is changed, a new average dc-side inverter voltage leads to a change in motor speed. Two types of closed-loop speed controllers were developed in the laboratory and are considered in this chapter. First, a closed-loop analog circuit is presented. The topology and operation of this circuit is carefully documented. Next, a digital signal processing (DSP) approach to the same control problem is outlined. The logic and structure of the DSP method are explained while an in-depth treatment of the dSPACE particulars is deferred until Chapter VIII.

B. ANALOG CONTROLLER OVERVIEW

In determining a closed-loop analog controller, the primary feedback signal is the machine speed (rpm) represented in the form of voltage. Naturally, most electrical controllers use voltage as the medium for control, so the initial thrust in the control effort was to implement the conversion from speed to voltage. This was achieved through the application of an optical encoder which converted the induction motor rpm into a TTL electrical signal. A microelectronics chip was then used to convert the variable TTL frequency to a variable dc voltage which was then fed back into the analog controller. As

discussed in the next section, the optical encoder signal had to be processed to properly interface with the microelectronics chip.

Once the proper speed voltage signal ($V\omega_{rm}$) was obtained, the closed-loop speed controller was designed and built with a series of op amps. The inputs to the control scheme included the rotor speed ($V\omega_{rm}$), the commanded rotor speed signal (V^*) and the nominal rotor speed voltage (V_{nom}). Safety features, including a voltage clamp and voltage limiter, were added to provide over-current protection. Figure 7.1 shows a block diagram of the analog circuit. Each block is dissected in the following sections.
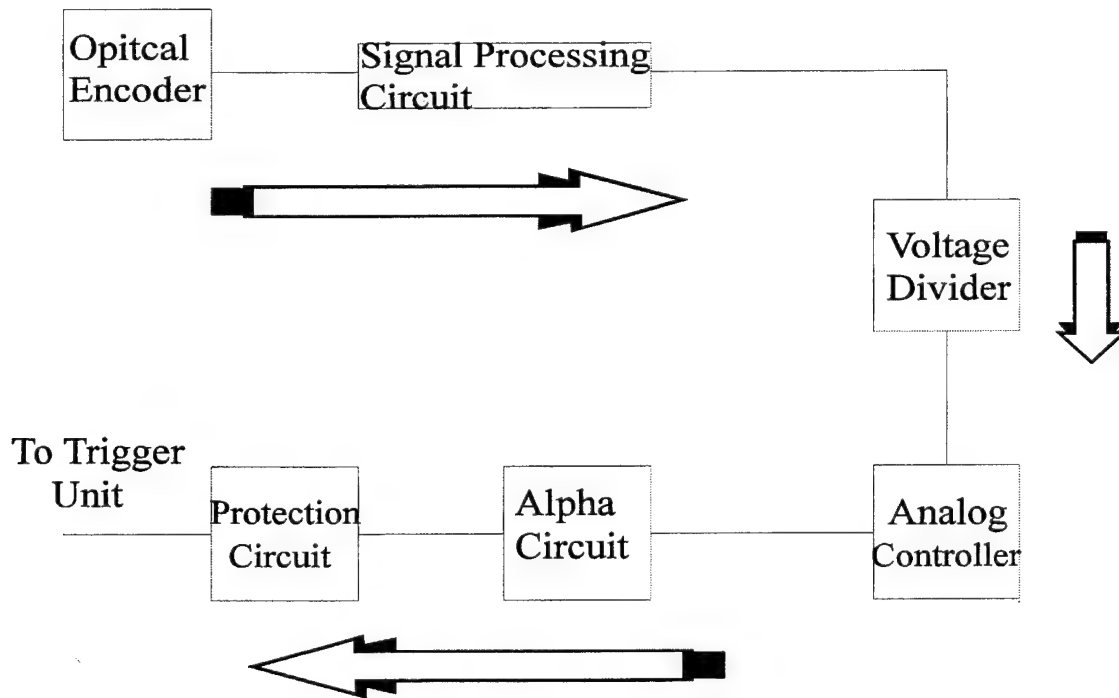
Figure 7.1 Block Diagram of Analog Circuit

C. SPEED REFERENCE SIGNAL

An optical encoder is a device that coverts the mechanical speed into an electronic signal. This is accomplished by attaching to the rotor an encoder wheel that has 1000 slots evenly-spaced about the periphery. The encoder wheel cuts perpendicularly through an emitter/detector arrangement that contains a photodiode. As the slots of the encoder wheel pass by the photodiode, pulses are generated from the emitter to the detector which are translated to a 0-5 volt TTL signal. Figure 7.2 shows the configuration used. A pull up circuit configuration was used to pull up the voltage values coming from the photodiode detector. A TTL signal from channel A was selected as the signal to represent the speed of the rotor. The channel B signal is ninety degrees out of phase with Channel A. Channel I is the index channel. It generates a pulse for every complete revolution of the encoder wheel.
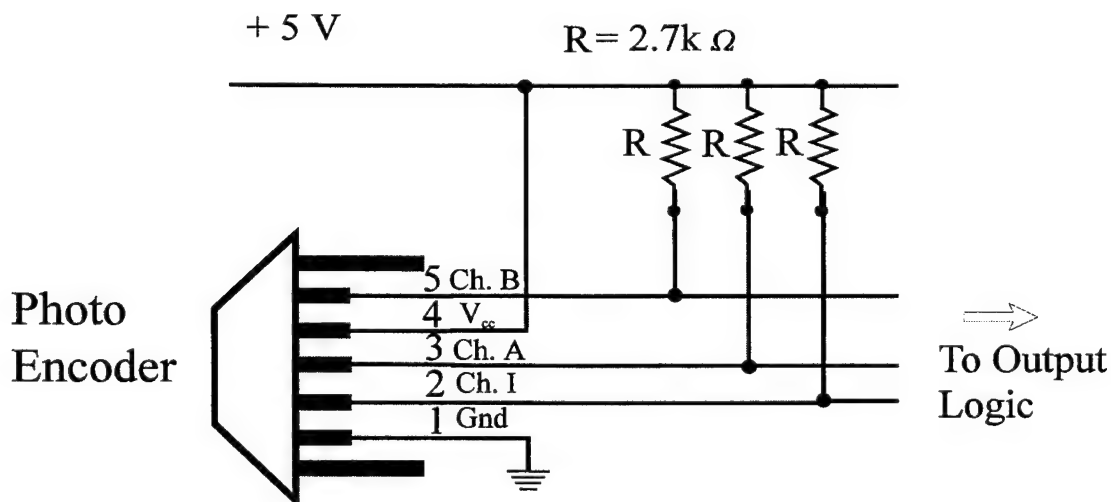
Figure 7.2 Optical Encoder Circuit

D. ENCODER SIGNAL PROCESSING

The firing control unit for the thyristor unit requires an external dc voltage to establish the firing delay. In this section, the approach used to convert the variable frequency pulse train of the optical encoder to a variable dc voltage is documented. This dc voltage is then available to a speed control circuit which generates the required voltage for the firing control unit. The first step involved processing the encoder signal so that a standard frequency-to-voltage conversion chip could be used directly. Figure 7.3 illustrates the circuitry used.

At low speed (830 rpm - maximum $\alpha=179.3°$), the frequency of the TTL signal from the encoder is 14kHz while at maximum speed, 1740 rpm ($\alpha=146.3°$), the frequency is 30kHz. Thus, the 14-30kHz interval is the nominal range of frequencies that the optical encoder generates. Due to the specifications of the frequency-to-voltage converter chip, LM2907, the encoder signal had to be processed.
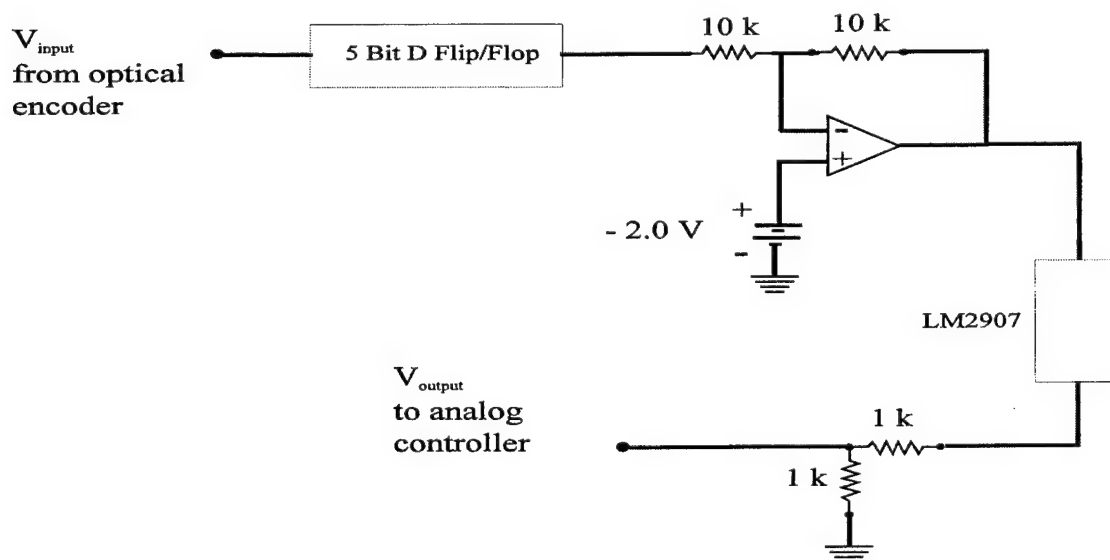
Figure 7.3 Signal Processing Circuit

The frequency limitations of the LM2907 chip required that the input frequency be scaled to a usable range. The input limit for the LM2907 is 1000 Hz, so the encoder frequency was stepped down through the use of a 5 bit D flip-flop arrangement. This is illustrated in Figure 7.3. This was accomplished by series connecting two 4-bit D flip-flop chips. As a result, the frequency range of the encoder signal was shifted to 430 - 935 Hz. The LM2907 is not compatible with a TTL signal, but it can process an appropriate square wave. A simple offset circuit shown in Figure 7.3 was used to change the TTL into a square wave signal with +/- 2.5 peaks. The resultant signal could now be inputted into the LM2907.

The dc voltage output of the LM2907 for the nominal operating range is 6.2 V for 830 rpm (430 Hz input signal) and 13 V for 1740 rpm (935 Hz input signal). Since the maximum permissible dc voltage required by the alpha control trigger unit is 10 V, this voltage range was scaled down to 3 to 6.5 V by a voltage divider network. The 3-6.5 V dc range is the voltage range the analog controller "sees" as an input representing the speed of the rotor. In the next section, the analog controller is discussed in detail.

After the signal is processed through the analog controller, the feedback signal goes through a circuit identified as the alpha circuit. Figure 7.4 illustrates this set-up. The purpose of the alpha circuit is to interface the controller output signal to the alpha control trigger unit. It accomplishes this with the Miller summer network shown. The Miller summer adds the weighted inputs into the op amp and outputs the negative of the sum. Each input is weighted or multiplied by the ratio of the feedback resistor (10k) to input resistor (10k). In the alpha circuit, inputs are the feedback voltage from the

71

controller (3 to 6.5 volts) and a constant -13.2 volts. At 830 rpm, the analog controller

delivers 3 volts to the alpha circuit. The output of the alpha circuit is then 10.2 volts. For

1740 rpm, the analog controller output is 6.5 volts and the alpha circuit output is 6.7

volts. Thus, the alpha circuit scales the controller output to the desired alpha range of

146.3° to 179.3°.

After the signal is translated by the alpha circuit, the feedback signal goes through

a protection circuit as illustrated in Figure 7.4. This circuit clamps the dc voltage values

that go to the alpha control trigger unit. This clamping is implemented with two voltage

limiters. The first voltage limiter prevents the dc voltage value from going below 6.3

volts; the second prevents the dc value from exceeding 10 volts. Recall, the 6.3 volts

corresponds to 146.3° while 10.0 volts corresponds to 179.3°. Thus, the alpha angle is

locked into the range of 146.3° to 179.3° so that a safe operating environment is ensured

for the SERS. Any alpha angle below 146.3° produces severe over-current situations and

damage to equipment may occur.
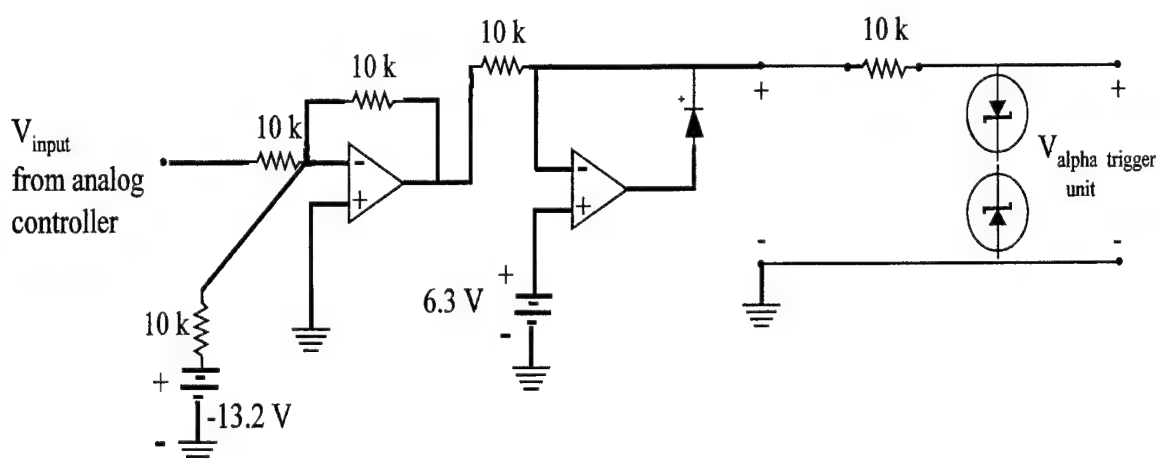
Figure 7.4 Alpha and Protection Circuits

72

E. ANALOG CONTROLLER

1. Description

The analog controller is a closed-loop controller composed of op amps and resistors with voltage inputs corresponding to the actual rotor speed and commanded rotor speed. The output is then sent to the thyristor control trigger unit via the alpha and protection circuits. Figure 7.5 illustrates the analog controller with the op amps numbered and the various signal points identified. For clarity, ω's(rotational speeds) are used instead of V's (voltages) in tracing the signals through the controller.

Figure 7.5 Analog Controller Schematic

The operation of the controller is best described by first considering the steady-state condition. For low-speed operation at 830 rpm, the voltage signal representing the

rotor speed is 3.0 volts. This is selected as being the nominal condition and changes in speed are referenced from this point. Thus, a separate 3 volt source is required to set this reference speed (voltage). Viewing Figure 7.5, this input is denoted in the far left of the figure and is represented as $\omega_{rm,nom}$.

Following the first op amp, the signal is inverted and becomes $-\omega_{rm,nom}$. The second input to the controller scheme is the actual speed of the rotor given in volts. The rotor speed signal in volts is processed through the optical encoder processing scheme as described earlier and is about 3 volts at 830 rpm. The processed rotor voltage signal representing rotor rpm is represented by ω_{rm} which is then inputted into the second op amp. The output of the second op amp is $\omega_{rm,nom} - \omega_{rm}$ which at nominal speed is approximately zero volts.

The inputs to the third op amp are the commanded rotor speed, given by $\Delta\omega_{rm}^{*}$, and the output from the previous op amp. In this example, the command signal is initially set to zero. The gain of the third op amp is set by the feedback resistor. By changing this feedback resistor, the transient response of the controller may be adjusted to provide a certain level of steady-state error, overshoot, or settling time.

The final op amp in the circuit sums the negative of the nominal speed together with the output of the previous op amp. For the steady-state example under consideration (830 rpm), the output of the fourth op amp is around 3 volts. After going through the alpha circuit, this is translated to just over 10 volts and is subsequently clipped to 10 volts even. Thus, the trigger unit receives a 10 volt signal and maintains the rotor speed at 830 rpm.

74

The transient operation of the control circuit is considered next. If it is desired for the machine speed to be increased, then an increase in $\Delta\omega_{rm}^*$ would be specified by increasing the voltage from the external dc source. The command specified voltage would then added to the steady-state output from op amp 2 which is zero. The output of the third op amp would be $-K_p\Delta\omega_{rm}^*$ or the negative of some factor times the commanded voltage value. The fourth op amp adds in the negative nominal voltage with the output of the previous op amp. Assuming $K_p=1$, the output of the fourth op amp is $\Delta\omega_{rm}^* + \omega_{rm,nom}$ which is equal to 1+3 or 4 volts.

The one-volt increase from the analog controller causes a corresponding one volt decrease (to 9.2 volts) in the signal to the trigger unit. The firing angle, α, decreases because of the decrease in the voltage signal to the trigger unit. Subsequently, the motor speed increases as desired. The increase in motor speed causes a slight increase in the ω_{rm} signal. The slightly greater values of ω_{rm} and the nominal voltage yield a small negative value of the output of the second op amp. For $K_p=1$, the output of the third op amp is a negative value of less magnitude than the previous time, and the fourth op amp yields a value slightly smaller than the last time, maybe 3.8 volts. This brings about a decrease in the motor speed which produces a decrease in the ω_{rm} signal. This causes the $\omega_{rm,nom} - \omega_{rm}$ signal to less negative which makes the output of the fourth op amp to be slightly more positive, maybe 3.85 V. This continues until equilibrium is reached or $\omega_{rm,nom} - \omega_{rm} + \Delta\omega_{rm}^* \approx 0$. When equilibrium is reached, the motor operates at a higher speed, and the feedback signal to the trigger unit is a steady value.

75

2. Performance

After constructing the analog controller and the alpha and protection circuitry, static testing with representative signals was conducted to ensure that the controller was working properly. Static testing included varying the command voltage input, measuring the trigger unit voltage levels and ensuring the alpha and protection circuits were working properly. In another test prior to controller installation, all aspects of the controller were connected except the final signal to the trigger unit. The induction machine was started and output levels to the trigger unit were measured. Alpha and the command voltage signal were varied by hand, and the trigger output signal was monitored. Static and semi-static test results were satisfactory.

Finally, the closed-loop controller was connected. When the induction machine starts up, $\alpha=154.0°$ because of the voltage low limiter. As rotor rpm increases, α increases and climbs to the specified value of 179.3°. When a command signal was initiated, the system responded as expected. Table 7.1 gives the specific data results.

As mentioned earlier, the feedback resistor for the third op amp was variable and two cases were considered. The first case included a 53k Ω resistor or $K_p=5.3$, and the second case included a 20k Ω resistor or $K_p=2.0$. The data in Table 7.1 show that the first case yields a greater alpha range for a given command voltage interval. Greater alpha range translates into greater range in rpm. Another observation is that for the second case, for the same speed range, the available command voltage range is larger. Thus, case 2 offers a larger dynamic range for the voltage input.

53K						
$\Delta\omega_{rm}^{*}$ (V)	$\omega_{rm,nom}$ (V)	ω_{rm} (V)	ω_{rm} (rpm)	To α ckt (V)	To trigger unit (V)	α angle (degrees)
0	2.976	2.947	820	2.632	10.29	179.3
0.5	2.976	3.349	930	3.751	9.462	175.1
1.0	2.976	3.791	1060	4.284	9.018	170.9
1.5	2.976	4.198	1170	4.678	8.540	166.6
2.0	2.976	4.611	1280	5.149	8.114	163.1
2.5	2.976	5.054	1410	5.580	7.666	158.9
3.0	2.976	5.444	1520	6.009	7.231	155.4
3.5	2.976	5.900	1650	6.447	6.821	151.2
4.0	2.976	6.215	1740	7.172	6.307	147.0
4.5	2.976	6.215	1740	10.208	6.307	147.0
20K						
$\Delta\omega_{rm}^{*}$ (V)	$\omega_{rm,nom}$ (V)	ω_{rm} (V)	ω_{rm} (rpm)	To α ckt (V)	To trigger unit (V)	α angle (degrees)
0	2.976	2.979	820	2.864	10.23	179.3
0.5	2.976	3.244	900	3.617	9.587	176.5
1.0	2.976	3.515	980	3.951	9.271	173.7
1.5	2.976	3.870	1075	4.337	8.875	170.2
2.0	2.976	4.206	1170	4.683	8.536	166.6
2.5	2.976	4.495	1250	5.004	8.231	163.8
3.0	2.976	4.887	1360	5.393	7.832	161.0
3.5	2.976	5.150	1440	5.702	7.547	158.2
4.0	2.976	5.510	1550	6.038	7.203	155.4
4.5	2.976	5.835	1630	6.405	6.848	151.9
5.0	2.976	6.177	1740	6.730	6.514	149.1
5.5	2.976	6.218	1740	7.647	6.304	147.0
6.0	2.976	6.217	1740	8.693	6.305	147.0

Table 7.1 Analog Controller Data

F. DSPACE CONTROLLER

1. Description

After verifying the satisfactory operation of the analog controller described above,

a dSPACE (digital signal processing and control engineering) controller was designed,

implemented and tested. Before describing the dSPACE controller, a brief description of

dSPACE is in order. dSPACE allows for external analog signals to be digitally processed

in a computer and then exported to the outside world. It uses MATLAB (The
MathWorks, Inc., 1992), SIMULINK (Hicklin, et al., 1992) and a dSPACE card. The
dSPACE development package facilitates the design and implementation of digital
controllers without requiring that actual C code be written. A detailed discussion
covering dSPACE is included in the next chapter.

The dSPACE controller for this research effort is illustrated in Figure 7.6.
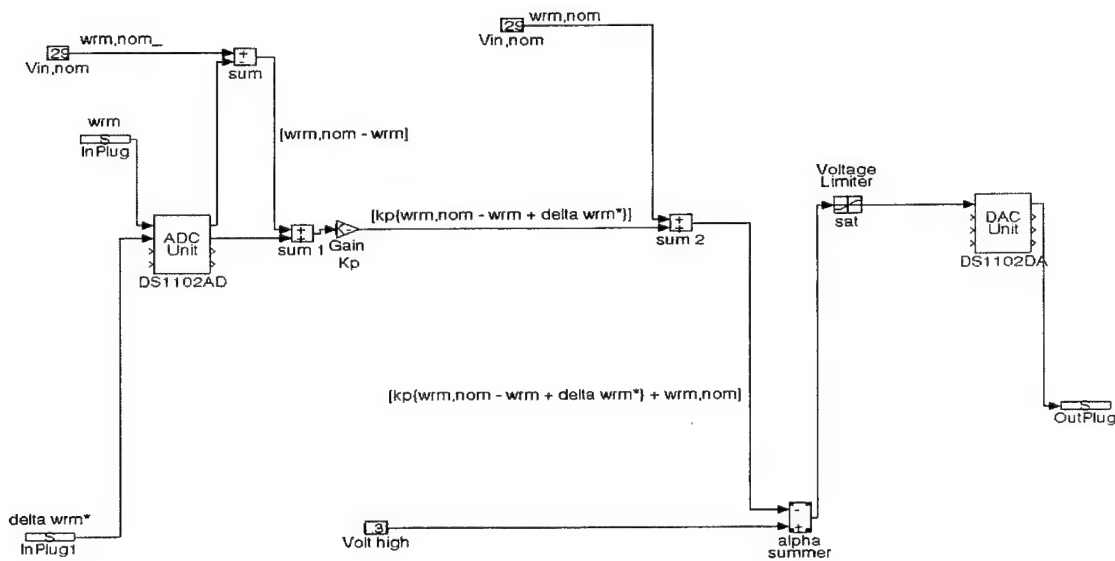
Figure 7.6 dSPACE Controller

The dSPACE controller is created in the SIMULINK environment. Once the
block diagram has been specified in an appropriate file, a command on a pull down menu
is executed and a C code model of the system depicted is automatically generated and
sent to the dSPACE board. With the microprocessor activated, the control algorithm is
initiated and real-time monitoring of various signals is possible. Using SIMULINK and
dSPACE icons, a controller similar to the analog controller was modeled. Testing was
done and a comparison to the analog controller was made.

78

Like the analog controller, the dSPACE controller is a closed-loop controller. Instead of op amps and resistors, it uses gain and summing blocks. The alpha circuit in the previous controller is modeled through a saturation block. External input voltages are replaced by constant value blocks. In the SIMULINK environment, the inplug/outplug ports the appropriate signals in and out of the dSPACE card. Conversion from analog to digital (A/D) and digital to analog (D/A) occurs in the blocks marked ADC Unit and DAC Unit, respectively. These blocks are conveniently provided in the dSPACE library.

In order to understand how this controller works, consider it in steady-state operation at 830 rpm. The rotating shaft produces a speed voltage via the optical encoder/signal processing circuitry. At 830 rpm, as in the previous controller, the voltage that represents ω_{rm} is about 3 volts. This signal is fed into the back of the computer through a synch terminal, ribbon panel and connector pins. The input signal, ω_{rm}, is automatically scaled down by a factor of ten so that it appears as 0.3 volts at the input plug. Following the same signal, it is converted into a digital signal and summed with $\omega_{rm,nom}$ which is represented by a constant 0.29 block.

At 830 rpm, the input measurement from the rotor speed voltage was observed to be about 0.29 volts, so for accuracy of the controller, the $V_{in,nom}$ block was changed to match the input rotor speed voltage.

Therefore, at steady-state nominal speed with no command signal, the output of the sum block is zero. The output of the sum1 block is also zero. The sum2 block will reintroduce the nominal speed voltage needed for steady-state operation. Similar to the previous controller, the alpha summer rearranges the signal for proper orientation for the

79

trigger unit. The alpha summer adds 1.32 to the negative of the incoming signal. For the nominal condition, 1.04 is the result which is sent to a limiter. The signal goes through a limiter with the upper limit of 1.0 and the lower limit of 0.7. After the limiter, the signal of 1.0 V is converted to analog and scaled to 10 volts. The output synch terminals are connected to the trigger unit and 10 volts yields a firing angle of 179.3°. Thus, steady-state operation is maintained.

To initiate a transient, an external analog dc voltage (command voltage) is connected to the synch terminal and processed in a manner similar to the rotor speed voltage. As shown in Figure 7.6, the command voltage enters through plug1. If the system is operating at steady-state 830 rpm and a 1 volt command signal is specified through inplug1, then the command voltage enters the SIMULINK circuit scaled down to 0.1 volt. After being converted in to a digital signal, $\Delta\omega_{rm}^{*}$ is added to the output of the summing block which at this point is zero. If K_p=1, then the output of block 2 is 0.39 volts (0.29 V + 0.1 V). After the alpha summer, the signal is converted to a new value of 0.93. Upon exiting the SIMULINK circuit, it is scaled to approximately 9.3 volts. As a result, the alpha angle decreases and the speed of the machine increases.

Once the speed of the machine increases, the rotor measured speed voltage increases, and the value injected into the SIMULINK circuit increases. This nonzero voltage forces the output of the summing block to go negative. The small negative number out of the summing block is added to the constant command signal to yield a smaller signal, perhaps 0.08 V, out of the sum1 block. After the sum2 block, the signal becomes slightly smaller than it was previously at the same location. This causes the

alpha angle to increase slightly which causes the machine to slow down. When the machine slows down slightly, the rotor speed voltage decreases slightly which causes the output of the sum block to become a smaller magnitude negative number. This causes the output signal of the sum1 block to be slightly greater than the previous signal for the same location. After the sum2 block and the alpha summer respond, alpha is decreased slightly causing the machine to increase in speed. This occurs until equilibrium is reached.

2. Performance

Prior to fully connecting the dSPACE controller, static testing was also conducted. First, the command voltage was varied and the output of the synch terminals was monitored for expected values. Secondly, the machine was started and the output of the synch terminals was monitored again. For both cases, the outputs were satisfactory indicating that the controller was operating as expected.

With preliminary testing finished, the composite controller placed in the loop by completing the connections between the synch terminals and the trigger unit. At steady-state and low speed, the alpha angle was 179.3°, and when the command voltage was varied via an external source, the system reacted as predicted.

For comparison purposes with the analog controller, identical test conditions were simulated using the dSPACE controller. Similar measurements were recorded and the data were contrasted.

In dSPACE, the signals in the controller may be traced continuously or for a specific period of time. These signals may then be viewed on the screen. During data

collection, the values for ω_{rm} (V) and voltage to the α circuit were obtained in this manner. It is important to note that the voltage values available inside dSPACE are scaled down by a factor of ten. The voltage to the trigger unit was measured by a fluke meter after the signal passed from the computer at the point just before it entered the trigger control unit. The commanded voltage, $\Delta\omega_{rm}^*$, was manually adjusted with an external dc voltage source. The value of K_p, the gain block in SIMULINK, was changed to model the change in feedback resistors as documented with the analog controller. Both runs were conducted and the measured data are included in Table 7.2.

The results measured for the dSPACE controller were found to be very similar to those obtained in the analog cases. The higher gain case, $K_p=5.3$, yielded a greater alpha range for a given command voltage range. As in the analog controller, the lower gain case offers a larger dynamic range for the voltage input. These findings mirrored those found for the analog controller.

Taking advantage of the versatility of dSPACE, an additional test was conducted on the dSPACE controller utilizing the trace window tool from dSPACE. Step changes in the command voltage and load were applied to the system for two cases, $K_p=5.3$ and 2.0. The results are shown in Figures 7.7 through 7.12.

Note in viewing Figures 7.7 through 7.12 that the signals traced inside the SIMULINK environment are scaled down by a factor of 10. For example in Figure 7.7, the 2.1 V step increase in command voltage is represented by a 0.21 V increase in command voltage in SIMULINK. The caption for Figure 7.7 reads "0.21 V Step Increase" when the external signal applied was 2.1 V.

82

Figure 7.7 Dspace Controller, K_p=2.0;
Voltage Output to Trigger Unit, V_{out},
Rotor Speed Voltage, V_{rm}, and
Command Voltage, V^*, (0.05V/div) vs.
Time (0.5sec/div) for 0.21V Step
Increase in Command Voltage

Figure 7.8 Dspace Controller, K_p=2.0;
Voltage Output to Trigger Unit, V_{out},
Rotor Speed Voltage, V_{rm}, and
Command Voltage, V^*, (0.05V/div) vs.
Time (0.5sec/div) for 0.21V Step
Decrease in Command Voltage

Figure 7.9 Dspace Controller, K_p=2.0;
Voltage Output to Trigger Unit, V_{out},
Rotor Speed Voltage, V_{rm}, and
Command Voltage, V^*, (0.05V/div) vs.
Time (0.5sec/div) for 3.2 lbf-in Step
Increase in Load, T_L

83
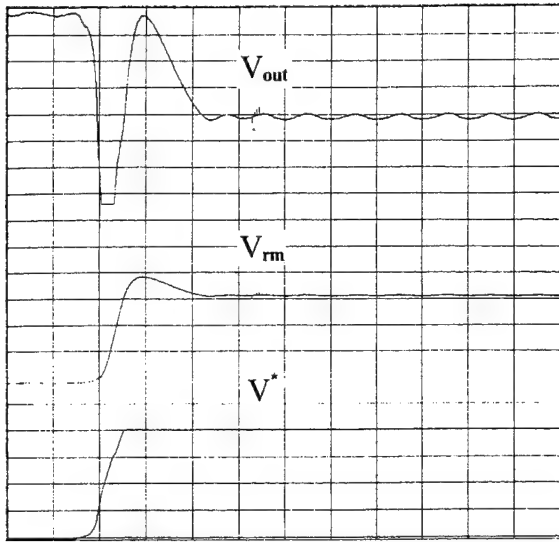
Figure 7.10 Dspace Controller, K_p=5.3;
Voltage Output to Trigger Unit, V_{out},
Rotor Speed Voltage, V_{rm}, and
Command Voltage, V^*, (0.05V/div) vs.
Time (0.5sec/div) for 0.21V Step
Increase in Command Voltage

Figure 7.11 Dspace Controller, K_p=5.3;
Voltage Output to Trigger Unit, V_{out},
Rotor Speed Voltage, V_{rm}, and
Command Voltage, V^*, (0.05V/div) vs.
Time (0.5sec/div) for 0.21V Step
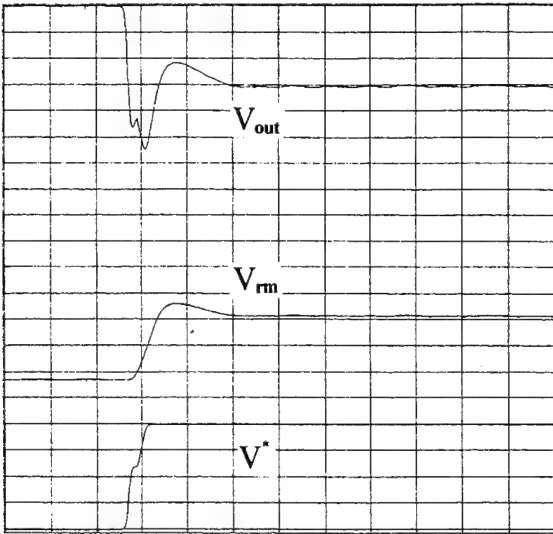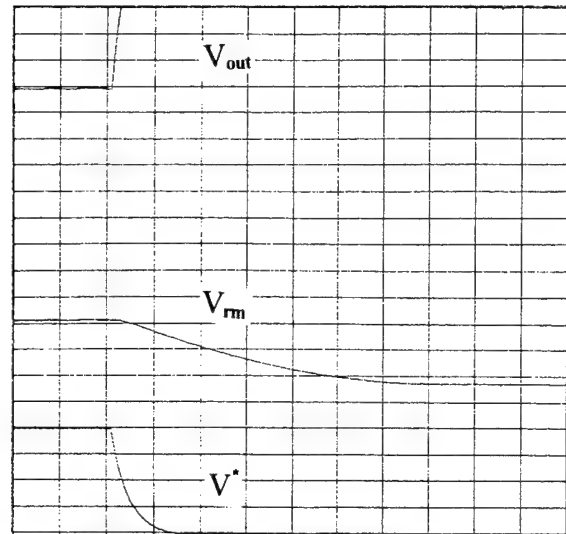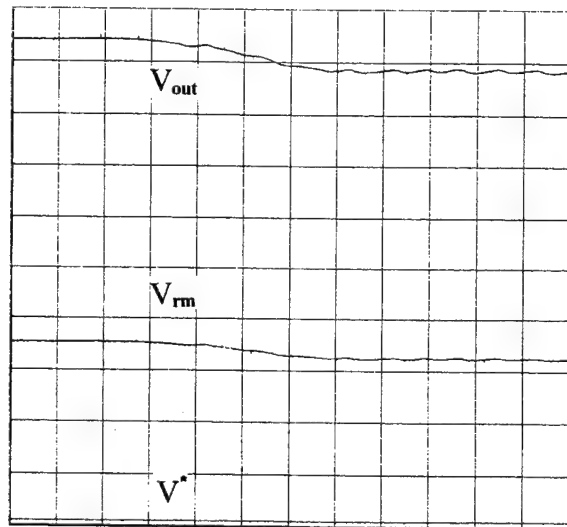Decrease in Command Voltage

Figure 7.12 Dspace Controller, K_p=5.3;
Voltage Output to Trigger Unit, V_{out},
Rotor Speed Voltage, V_{rm}, and
Command Voltage, V^*, (0.05V/div) vs.
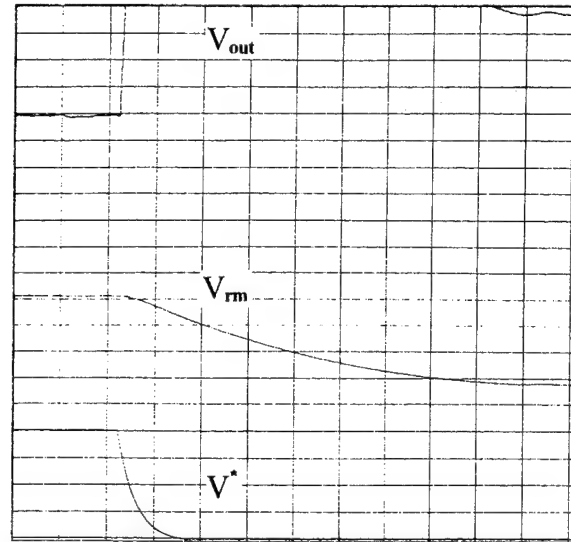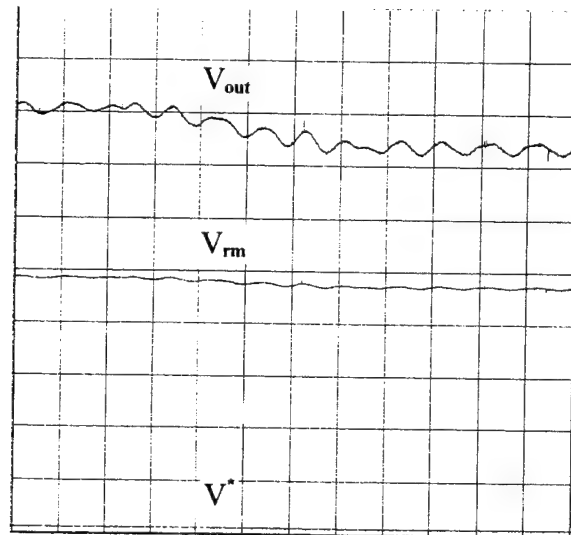Time (0.5sec/div) for 3.2 lbf-in Step
Increase in Load, T_L

84

$\Delta\omega_{rm}^*$ (V)	$\omega_{rm,nom}$ (V)	ω_{rm} (V) Inplug	ω_{rm} (rpm)	To α summer (V)	To trigger unit (V)	α angle (degrees)
			$K_p = 5.3$			
0	0.29	0.28	840	0.35	9.8	178.6
0.5	0.29	0.33	970	0.386	9.376	174.4
1.0	0.29	0.372	1090	0.433	8.87	170.2
1.5	0.29	0.412	1200	0.478	8.411	165.9
2.0	0.29	0.446	1300	0.516	8.06	162.4
2.5	0.29	0.483	1420	0.557	7.65	158.9
3.0	0.29	0.539	1540	0.6	7.24	155.4
3.5	0.29	0.565	1660	0.639	6.75	151.2
4.0	0.29	0.594	1740	0.728	6.30	147.0
4.5	0.29	0.593	1740	0.973	6.30	147.0
			$K_p = 2.0$			
0	0.29	0.282	820	0.326	9.96	179.3
0.5	0.29	0.314	940	0.365	9.55	175.8
1.0	0.29	0.341	1000	0.403	9.17	173.0
1.5	0.29	0.373	1100	0.436	8.85	170.2
2.0	0.29	0.402	1180	0.470	8.54	166.6
2.5	0.29	0.433	1270	0.499	8.21	163.8
3.0	0.29	0.462	1360	0.537	7.83	161.0
3.5	0.29	0.488	1450	0.568	7.53	158.2
4.0	0.29	0.519	1530	0.595	7.26	155.4
4.5	0.29	0.549	1620	0.624	6.97	152.6
5.0	0.29	0.578	1700	0.660	6.60	149.8
5.5	0.29	0.590	1750	0.731	6.30	147.0
6.0	0.29	0.590	1750	0.817	6.30	147.0

Table 7.2 dSPACE Controller Data

Viewing Figures 7.7 through 7.12 shows that the $K_p=2.0$ case is the more stable of the two cases. In the $K_p=5.3$ case, the steady-state output from the outplug has a superimposed oscillation; its response to the step load change contrasts sharply to the case with $K_p=2.0$. Graphically, it is apparent that $K_p=2.0$ yields a more stable response at

the expense of some steady-state accuracy. The speed variation when adding a step increase in load is illustrated in Figures 7.9 and 7.12. With K_p=2.0, rotor speed initially was 1400 rpm, and when the load was added, it decreased to 1350 rpm. With K_p=5.3, rotor speed initially was 1600 rpm, and when the load was added, it decreased to 1560 rpm. The speed variation with K_p=5.3 was shown to be smaller. dSPACE provides the capability to readily consider other more sophisticated controllers to improve the steady-state and transient responses.

3. Comparison

A comparison of the data measured for the two controllers reveals that for the same gain values, the dSPACE and analog controller measured values tracked closely. Changing the gain produced the same effects in both controllers. Signal values for both controllers match well, and the dSPACE model proved to be a good representation of the analog controller.

G. CONCLUSION

Two types of controllers were tested in the SERS. In each case, two values of gain were used to evaluate the system response. For each controller, the system responded in a similar manner for the given gains. From the dSPACE controller traces, it became apparent that the lower gain value provided more stability.

86

VIII. DSPACE

A. INTRODUCTION

A detailed description of the dSPACE hardware and software tools is presented in this chapter together with an example on how to apply these tools to the SERS problem. The dSPACE hardware and software tools allow for real-time interface between a personal computer and external machine configurations (electric machines, power electronics, etc.). dSPACE accomplishes this through the integrated application of a specific dSPACE microelectronic chip, the Texas Instruments C compiler (Texas Instruments, Inc., 1991), SIMULINK, and MATLAB. The final result is that a computer can be conveniently incorporated into the hardware loop making the system readily reconfigurable and flexible.

B. DSPACE OVERVIEW

dSPACE (digital signal processing and control engineering) is a technology that allows for processing, analysis and control of digital signals. It has the capability of digitally representing analog signals, modifying these signals through a control algorithm, and converting them back into an analog form. All this is accomplished in the computer.

For example, the dSPACE system may be used to monitor an external voltage which may represent speed or position (open loop) or it may be used as a controller, processing an external voltage and supplying a corrective signal to adjust speed or position through a feedback signal (closed loop) derived and implemented in the SIMULINK environment.

In a typical application, a controller or monitoring scheme is first constructed in the SIMULINK environment via MATLAB. Once the controller or monitoring scheme is designed, C code is automatically generated, and a C code model of the controller or monitoring scheme is sent to a real-time interface configuration located on the dSPACE card. At this point, the microprocessor is enabled and is ready to receive signals and transmit signals to the outside world. Input signals from the external hardware are transmitted via a synch connector panel, ribbon cable and 48 pin connector to the dSPACE card which is then made to connect with the C code model. Signals in the controller may be monitored in the trace window of the dSPACE tools icon. Continuous or static monitoring is available in the trace window. In addition, data may be sent and stored in a MATLAB file for later use.

In this research effort, the dSPACE card used was the DS1102 control board. Installation of this board involved the following issues: ensuring that the computer meets the board's operating requirements, setting the address location dip switches on the board in the proper position, and ensuring that the host interrupt lines are not connected.

The board will draw up to 2 amps on the 5 volt line and 100 ma on the +/- 12 volt lines from the host computer's power supply. The DS1102 board is used with the 386/486 based IBM computers and needs a 6.2" standard slot with a 16 bit connector.

The address location on the board is set at the factory. The dip switches should read the following order 1-8: on, on, off, off, on, on , on, and on. This gives the proper address to the board and provides continuity with the dSPACE software. The software associated with dSPACE looks for specific addresses in the computer architecture, and by

having the dip switches set in the proper configuration, the dSPACE software is compatible with the DS1102 control board.

The host lines which may be used as interrupts in system are left unconnected on the DS1102 board. From the factory, the host lines are not connected and leaving them as they are will ensure proper operation of the card.

After powering down the computer, the slot cover may be removed and the control board placed into the 16-bit slot. The board is secured by screwing in the slot bracket in the computer frame. Upon installation, the board is ready for use.

C. SOFTWARE REQUIREMENTS

Prior to starting any application of dSPACE, verification of the software installed on the personal computer is advised in order to ensure proper interaction between dSPACE, SIMULINK, and MATLAB. The correct versions of each software component must be installed in order to use dSPACE. For the dSPACE card installed in the Power Systems Laboratory, the user must log into the computer, open a widow, and invoke MATLAB. The quickest way to then verify the versions loaded on the computer in use is to type *ver* at the prompt in the MATLAB environment. The returned information will supply the software data installed. Also, the dSPACE key must be enabled in the back of the computer which allows access into the dSPACE environment. Without it, the system will not work.

In this research effort, the hardware and software components utilized in relation to dSPACE applications were as follows: a DS1102 control board for the dSPACE card, MATLAB 4.0, SIMULINK C Code Generator version 1.0.1 Beta, SIMULINK Model

89

Analysis and Construction Functions version 1.2d, SIMULINK Block Library version 1.2d, Control Systems Toolbox version 3.0b, Signal Processing Toolbox version 2.0b, and Nonlinear Control Design. Having the proper versions of these tools is essential for properly operating the dSPACE card.

The DS1102 control board is the actual microprocessing hardware unit used in this application. MATLAB is the analysis language that is used to invoke the SIMULINK environment where signals are monitored and processed. The SIMULINK C Code Generator generates and builds the C code model of the figure constructed in the SIMULINK environment when the proper command is executed. SIMULINK Model Analysis and Construction Functions contains the simulation algorithm (Euler, Runge-Kutta) and construction data (open, closed system) needed for building and investigating the SIMULINK model. The SIMULINK Block Library contains all the icons available for use in SIMULINK. The Control Systems Toolbox contains functions such as model building, conversion and reduction. It also contains control functions for time and frequency responses, gain selection, root locus and equation solution. The Signal Processing Toolbox contains functions (i.e. Butterworth and Chebyshev filters) which are commonly used in signal processing applications. Nonlinear Control Design uses functions which enable the simulation of nonlinear aspects of control systems.

After installing or ensuring that proper versions of MATLAB, SIMULINK, MS-Windows and MS-DOS software are loaded on the computer, the steps listed below should be taken to properly load the dSPACE software. All the diskettes needed for software installation are located in the Power Systems Laboratory at NPS.

1. For the C code compiler, install TMS320 software tools on a created directory c:\c30tools. Install all 5 disks on the same directory. Use the following procedure: create a directory to contain the C compiler by entering MD C:\c30tools, copy the disks on the C drive by the command *COPY A: *.** *C:\c30tools*.**, repeat the copy command for each disk.
2. Install LD31 software and create the directories c:\dsp_cit\exe and c:\dsp_cit\citfiles.
3. Install slave applications. (c:\dsp_cit\slave)
4. Install CLIB software. (c:\dsp_cit\clib1102)
5. Install TRACE software. (c:\dsp_cit\)
6. Install SIMULINK C Code Generator using *a: setup* command.
7. Install RTI31 software. (c:\dsp_cit\)

D. EXTERNAL INTERFACE

1. Overview

The DS1102 control board contains several Input/Output (I/O) units: digital to analog (D/A) and analog to digital (A/D) converters, Bit I/O in/out unit, encoder phase lines unit and a pulse width modulation (PWM) unit.

This library is accessed by entering the c:\matlab\toolbox\user\dspace\dcdc directory. Once there and upon opening a MATLAB command window, the user must type *simulink* at the MATLAB command prompt. This will cause the SIMULINK library to appear on the screen. Upon opening a new file in the SIMULINK command window, the user will open the SIMULINK workspace window needed for modeling. By returning to the MATLAB command window and typing *ds1102* and *plugs* at the MATLAB command prompt, the user is provided icons needed for the DS1102 control board function. The SIMULINK library icons supplement these DS1102 I/O units. The SIMULINK icons are accessed by "double clicking" on one of the seven icons found in the SIMULINK command window. The desired icons may then be "clicked" upon and

91

dragged from either the SIMULINK, DS1102 or plugs libraries to the SIMULINK environment workspace.

A signal in the SIMULINK environment is monitored in the trace window. To begin tracing a signal, *trace 31* must first be accessed in the dSPACE tools icon. Before commencing a trace, the user must ensure that the corresponding map file is loaded in the trace window. This is done by entering the file pull down menu of the trace command window and ensuring the map file has the same name as the SIMULINK model where the desired tracing is to take place. Automatic tracing or tracing for a specific amount of time can be accomplished by selecting the desired signals to be traced, specifying the length of time for the trace and "clicking" upon the *start* button. The trace is viewed by entering the plot pull down menu and "clicking" on *trace plots*.

The plugs library provides the input/output icons that are used in the SIMULINK environment and that represent the various connector pins (48 available in all) located on the back of the computer. These connector pins are connected to a ribbon cable which is attached to the terminal of a synch connector. Also attached to the synch connector terminals are actual wires used to receive/send signals to any hardware that may be involved.

2. Input/Output Connector Pins

Each I/O connector pin is associated with a specific function in the DS1102 library of icons. In dSPACE (1993), the I/O connector pin designation is displayed on page 55. On a one-for-one basis, each connector pin has a corresponding synch

connector terminal to which it is attached via a ribbon cable. These corresponding connections are listed in the Appendix.

For example, suppose one wants to trace an analog signal using dSPACE. The ac signal would be applied to a synch connector terminal with the signal being attached to terminal one and the ground being attached to terminal two. This signal is transmitted through the ribbon cable to the corresponding pins, one and 22 respectively. In the SIMULINK environment, the user must have one input plug from the *plugs* library connected to an A/D converter which must be connected to an output plug or port. A distinction must be made between an output plug and port. An output plug delivers the signal to the connector pins, and an output port delivers the signal to the SIMULINK environment.

Continuing with this example, if one wanted to see this signal processed by dSPACE and the output sent from the computer to an oscilloscope, then, in the SIMULINK environment, the A/D converter needs to be attached to a D/A converter which is connected to an output plug. In this case, connector pins 15 and 43 are used (see Appendix A) which correspond with synch terminals 17 and 18. Connecting the oscilloscope terminals to the wires emitting from synch terminals 17 and 18, allows the user to view the analog signal on the oscilloscope window.

E. DSPACE CAPABILITY

The DS1102 library has numerous icons that support the variety of functions associated with the DS1102 control board. In this section each icon is explained and the various limitations revealed.

The 4-channel A/D converter is represented by the DS1102AD icon. Its first two channels have 16-bit resolution while its last two have 12-bit resolution. Input signals can range from -10 to 10 volts, and corresponding output signals are scaled to range from -1 to 1 volt.

The 4-channel D/A converter with 12-bit resolution is represented by the DS1102DA icon. The input signals are scaled to a range of 1 to -1, and the output signals have a range of 10 to -10 volts.

The 4 or 6-channel PWM signal generator with selectable resolution is represented by the DS1102PWM icon. Input signals are scaled to a range of -1 to 1 volt which ranges from 0-100% duty cycle. The output signal is a TTL type PWM signal. If four of the six channels of the PWM are used, then the resulting signal generation occurs in the first four channels. If channel 5 or 6 is used, then 6-channel signal generation occurs. Resolution for the PWM is selectable by "clicking" on the icon's dialog box. It can range from 8 to 14-bit resolution.

The DS1102 Bit I/O Unit for Digital Inputs is represented by the DS1102IN icon. This icon can be used to receive or send bit streams. It receives a TTL type signal from a multiplexed input plug. Its output signal is one, if a bit is set, otherwise it is a zero. The DS1102 Bit I/O for Digital Outputs is represented by the DS1102OUT icon. For an input signal not equal to zero, the bit is set. Its output signal goes to a multiplexed output plug which yields a TTL type signal. For any application, the number of input lines used in the DS1102IN plus the number of output lines used in the DS1102OUT must not exceed

16. I/O lines 1-16 correspond to I/O pins 0-15 (see page 55 of dSPACE (1993)).

Different channel numbers must be used for all I/O lines.

The DS1102 Encoder Phase Lines Unit is represented by the DS1102ENC icon. It provides a position value for two encoder interface input channels. It receives a signal from an input plug, and its output plug is scaled to -1 to 1 volt. The encoder contains a 24-bit counter which counts the number of pulses entering through the input plug. The differential mode of operation, which is the nominal mode, requires that a single input is connected to a single phase of the optical encoder which provides absolute position. Another application of the DS1102ENC icon is that of a speed monitor. This is accomplished by providing 1.5 volts dc to the pins of the channel of the encoder that is not being used and applying the optical encoder TTL signal to the channel in use. The index signal of the encoder zeroes the 24-bit counter, and as pulses enter DS1102ENC, the count increases. The DS1102ENC outputs a value corresponding to the number of pulses received, and then the counter is reset to zero. This feature is good for developing a measure of the speed (rpm) of an electric machine given an optical encoder output.

F. SIMPLE SET-UP

1. Example

In this section, a simple set-up is introduced and the procedures for running it are presented. In this example, an analog ac signal is inputted to dSPACE, monitored by the computer and then delivered back to an external oscilloscope.

A 5 volts peak-to-peak ac signal is attached to terminals 1 and 2 which correspond to connector pins 1 and 22 via the ribbon cable. Signals from the dSPACE card are

delivered from connector pins 15 and 43 through the ribbon cable to corresponding terminals 17 and 18 to the oscilloscope terminals and then are viewed on the oscilloscope screen.

In the Windows environment, the user should "double click" the MATLAB Codegen icon. In the MATLAB command window, the user should then "click" *open m-file* in the file pull down menu and access the directory c:\matlab\toolbox\user\dspace\dcdc. Once in this directory, the user must "click" *cancel*, and the MATLAB command window should be viewed. Next, the user must type *simulink* at the MATLAB command prompt, and the SIMULINK library should appear.

In the SIMULINK window, under the file pull down menu, the user must open a new file by "clicking" *new* which will provide the work environment for the icons. Returning to the MATLAB command window, the user then must type *ds1102* and *plugs* at the MATLAB command prompt which will provide icons needed to complete our example. "Click" and drag from the plugs library input and output plugs icons and deliver them to the SIMULINK environment. From the DS1102 library, the user should "click" and drag A/D and D/A converters icons and deliver them to the SIMULINK environment. The components must be arranged and connected in the following manner: input plug, A/D converter, D/A converter and output plug. The connections are made by starting on the edge of the input connection, "clicking" and "holding" the left button on the mouse, dragging the line to the A/D converter channel one (the uppermost one) and releasing the button. This completes the connection between the input plug and the A/D converter. The rest of the connections are similarly made. Having made the proper

connections, the user may then enter the simulation pull down menu and "click" *parameters*. At this point, the start and stop times, minimum and maximum step size and return variable may be adjusted as needed. For example, reasonable values for start and stop times, minimum and maximum step size and return variable are 0, 0.1, 0.001 and 1.0, time, respectively. The user must next save this file as a m-file by "clicking" *save as* in the file pull down menu in the SIMULINK window. In recalling the file for future work, all one has to do is type the file name minus the suffix at the MATLAB prompt in the MATLAB command window.

To activate the dSPACE card and generate the C Code model, the user must "click" *Generate and Build Real-Time* in the Code pull down menu. An active real-time interface window will appear which will turn to an inactive status after compilation is completed. After compilation, the user must close this window. The digital signal processor (DSP) has started.

In the dSPACE tools icon, the user should "double click" *trace 31*. This provides access to the trace window environment where signal tracing takes place. In the trace window environment, the file pull down menu is entered to ensure that the proper map file is being used in the trace window. The file name should be the same as the file name used in the SIMULINK environment except the suffix is ".trc" vice ".m". Once the proper file is selected, the user must return to the trace window and select the signals desired to be traced and the interval desired. The user should then "click" the *start* button and the tracing commences. Upon entering the plot pull down menu, the user must "click" on *trace plots* to view the real-time plots. Signals can be viewed externally on the

97

oscilloscope window and on the trace window. To return to the trace window, the trace pull down menu is entered and the user "clicks" on *control panel*. To close the trace window, the file pull down menu is entered and the user "clicks" on *close*.

If the MATLAB command window is closed, then the SIMULINK environment window will close also. To stop the DSP, the user must "click" on the *DOS prompt* icon in the main menu icon then type *ld31* at the DOS prompt. Finally, the user must type *q* to quit.

2. Precautions

Two precautions are necessary before beginning work with the dSPACE. The first is to ensure strict adherence to proper grounding procedures. Circulating grounds may cause damage to the dSPACE card. Generally, the circuit board is referenced to ground and that ground is connected to all other grounds. This ensures that there is only one ground. The second precaution is voltage and current isolation. High voltage conditions (>10 volts) may cause damage to the dSPACE card. All signals coming into the dSPACE card should be voltage limited. Figure 8.1 illustrates such a voltage limiter. Signals emitting from the dSPACE card should be configured like Figure 8.2 in order to prevent a reverse current situation. The cheaper op amp will be sacrificed instead of the expensive dSPACE card.

G. CONCLUSION

The dSPACE hardware and software tools offer a real-time interface between a personal computer and external machine configurations. Through the coordination of

several languages and the dSPACE card, dSPACE provides a different approach in the monitoring and controlling of signals in various controller schemes.
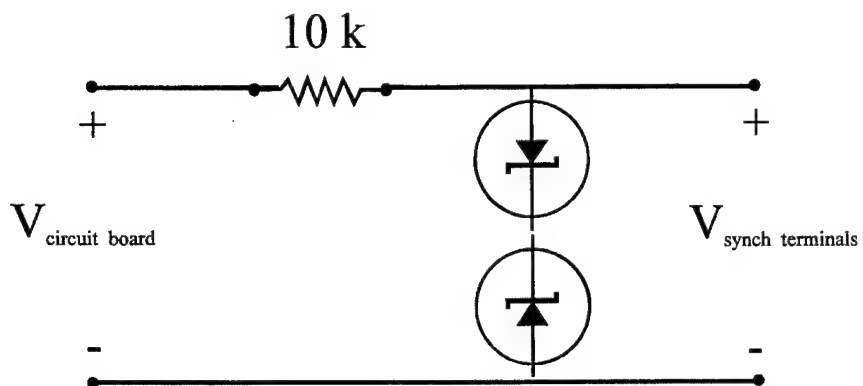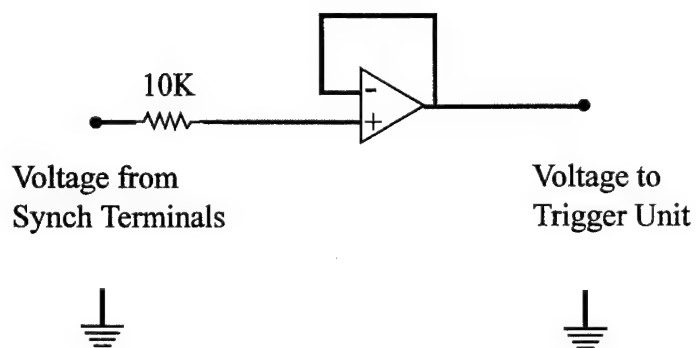

Figure 8.1 dSPACE Protection Circuit

Figure 8.2 dSPACE Protection Circuit

IX. CONCLUSION

A slip energy recovery system (SERS) offers an alternative approach for induction machine speed control. For a narrow range of speed control, the SERS is more efficient than an equivalent variable rotor resistance scheme, and the power electronics are significantly less expensive than an equivalent stator voltage control scheme. As such, this drive is popularly used in a multitude of fan and pump applications. Considering the push toward using more electric components in naval combatant ships, the variable speed capabilities of the SERS may make it an attractive alternative to present-day fixed-speed drives. It may be found that operating certain loads at variable speeds may enhance the performance of the equipment or improve the efficiency.

The work reported on in this thesis has sought to validate the operation and control of a 1/4 horsepower SERS. The basic theory underlying the SERS as well as a steady-state analysis has been presented as a means of verifying the hardware operation. Several preliminary configurations were considered to both investigate the hardware limitations and to assess a baseline drive that could then be used for further study. In determining the baseline configuration, it was found that the location of the transformer significantly impacted the performance of the drive. In order to obtain a wide range of speed values, it was decided to situate the transformer between the rotor and the diode bridge.

Upon developing the hardware implementation of the baseline SERS, detailed studies of signal waveforms, power flow, and efficiency were performed. In addition, a

correlation was made between the theoretical analysis and the collected data. The power flow was found to reflect the analysis trends well. The analysis of the link voltages and the rotor speed were also found to closely match the theory as long as the resistance of the inductor was taken into account. The gains in efficiency were not as apparent, as most of the case studies were performed with less than half full-load torque.

An analog and a computer-based feedback control system were next developed and implemented. The analog design required installing an optical encoder, interfacing the output of the encoder to a frequency-to-voltage conversion chip, and then processing both the speed command and speed feedback signals through a proportional controller implemented with several op amps. The purpose behind generating an analog controller was to acquire a reliable scheme before extending the concept to a more critical microprocessor system.

A significant effort was next placed into converting the analog design into an equivalent microprocessor design. The dSPACE development package in the Power Systems Laboratory consists of a set of hardware and software tools which facilitate the largely graphical design of digital interface systems. This thesis has clearly documented how to install the necessary software and the dSPACE board, how to correctly import and export signals to and from the board, how to construct simple control systems in SIMULINK, how to automatically generate C code and start the microprocessor running, and how to monitor on-screen the variation of selected variables. It is hoped that the extensive documentation will aid in future dSPACE endeavors.

Both controllers were found to perform adequately though additional research into more advanced control structures may yield improvements. Examples may include PI-speed controllers or a controller which attempts to also regulate the dc link current.

The SERS research documented in this thesis has gone into considerable detail, however, many avenues for continued research exist. In particular, the digital modeling and reduced-order modeling of the SERS would be facilitated by the data and waveforms presented here. Also, further control development would be aided by the information presented on the analog and dSPACE controllers. Finally, a critical assessment of the location of the transformer based on power factor and efficiency criteria can be performed in order to optimize its location.

APPENDIX.   I/O CONNECTOR/TERMINAL PINOUT

Signal	Connector Pin	Synch Terminal
ADC 1	1	1
Analog Ground	22	2
ADC 2	2	3
Analog Ground	23	4
ADC 3	3	5
Analog Ground	24	6
ADC 4	4	7
Analog Ground	25	8
IOP1 (2)	7	9
IOP3 (4)	8	10
IOP5 (6)	9	11
IOP7 (8)	10	12
IOP9 (10)	11	13
IOP11 (12)	12	14
IOP13 (14)	13	15
IOP15 (16)	14	16
Digital Ground	15	17
DAC 1	43	18
Digital Ground	26	19
DAC 2	44	20
Digital Ground	60	21
DAC 3	45	22
Digital Ground	47	23
DAC 4	46	24
Phi90 2	16	25
Phi0 2	17	26
Index 2	18	27
/Phi90 2	37	28
/Phi0 2	38	29
/Index 2	39	30
IOP0 (1)	28	31
IOP2 (3)	29	32
IOP4	30	33
IOP6	31	34
IOP8	32	35
IOP10	33	36
IOP12	34	37
IOP14	35	38
CAP0	50	39
CAP1	51	40
CAP2	52	41
CAP3	53	42
CMP0	54	43
CMP1	55	44
CMP2	56	45
CMP3	57	46
Vsupply	61	47
Vsupply	62	48

LIST OF REFERENCES

Akpinar, E., Pillay, P., and Ersak, A., "Starting transients in slip energy recovery induction motor drives," *IEEE Transactions on Energy Conversion*, vol. 7, no. 1, pp. 245-251, Mar. 1992.

Arsenault, B., Lab Volt Systems, Quebec, Canada, telephone conversation, Jun. 1995.

Borges da Silva, L.E., Lambert-Torres, G., Ferreira da Silva, V., Nakashima, K., April, G.E., and Olivier, G., "Adaptive fuzzy techniques for slip-recovery drive control," *IEEE International Conference on Fuzzy Systems*, pp. 381-388, Mar. 1992.

dSPACE digital signal processing and control engineering GmbH, *DS1102 User's Guide*, Document Version 2.0, Paderborn, Germany, 1993.

Dubey, G.K., *Power Semiconductor Controlled Drives*, Prentice-Hall, Inc., Englewood Cliffs, NJ, 1989.

Hicklin, J., Grace, A., Packer, D., Packard, C., de Rienzo, J., and Little, J., *SIMULINK Dynamic System Simulation Software User's Guide*, The MathWorks, Inc., Natick, Massachusetts, 1992.

Hildebrandt, M.S., *Reference Frame Theory Applied to the Analysis of a Slip-Recovery System*, Master's Thesis, Department of Electrical Engineering, Purdue University, Dec. 1986.

Krause, P.C., Wasynczuk, O., and Sudhoff, S.D., *Analysis of Electric Machinery*, McGraw-Hill, Inc., New York, 1986.

The MathWorks, Inc., *MATLAB High-Performance Numeric Computation And Visualization Software Reference Guide*, The MathWorks, Inc., Natick, Massachusetts, 1992.

Miles, A.R., "Transfer functions of the slip-controlled induction machine," *IEEE Transactions on Industry Applications*, vol IA-15, no. 1, Jan. 1979.

Refoufi, L., Pillay, P., and Harris, M.R., "A step-down chopper-controlled slip energy recovery induction motor drive," *IEEE Transactions on Energy Conversion*, vol. 8, no. 3, pp. 396-403, Sept. 1993.

Smith, G.A. and Stephens, R.G., "Power factor control in a slip energy drive," *Fourth International Conference on Power Electronics and Variable-Speed Drives*, pp.353-357.

Stemmler, H., "High-power industrial drives," *Proceedings of the IEEE*, vol. 82, no. 8, pp. 1266-1286, Aug. 1994.

Texas Instruments, Inc., *TMS320 Floating-Point DSP Optimizing C Compiler User's Guide*, Texas Instruments, Inc., Houston, Texas, 1991.

INITIAL DISTRIBUTION LIST

1. Defense Technical Information Center..2
   8725 John J. Kingman Rd., STE 0944
   Fort Belvoir, Virginia 22060-6218

2. Library, Code 13..2
   Naval Postgraduate School
   Monterey, California 93943-5101

3. Chairman, Code EC 1
   Department of Electrical and Computer Engineering
   Naval Postgraduate School
   Monterey, California 93943-5121

4. John Ciezki, Code EC/Cy..1
   Department of Electrical and Computer Engineering
   Naval Postgraduate School
   Monterey, California 93943-5121

5. Robert Ashton, Code EC/Ah...1
   Department of Electrical and Computer Engineering
   Naval Postgraduate School
   Monterey, California 93943-5121

6. Brian S. Tait..1
   c/o Carol Tarkington
   1522 West Queen St.
   Edenton, North Carolina 27932